symmetry

Article

Analytical Investigation of the Heat Transfer Effects of Non-Newtonian Hybrid Nanofluid in MHD Flow Past an Upright Plate Using the Caputo Fractional Order Derivative

N. M. Lisha and A. G. Vijayakumar *

Department of Mathematics, School of Advanced Sciences, Vellore Institute of Technology, Vellore 632014, India
* Correspondence: vijayakumarag@vit.ac.in

Abstract: The objective of this paper is to examine the augmentation of the heat transfer rate utilizing graphene (Gr) and multi-walled carbon nanotubes (MWCNTs) as nanoparticles, and water as a host fluid in magnetohydrodynamics (MHD) flow through an upright plate using Caputo fractional derivatives with a Brinkman model on the convective Casson hybrid nanofluid flow. The performance of hybrid nanofluids is examined with various shapes of nanoparticles. The Caputo fractional derivative is utilized to describe the governing fractional partial differential equations with initial and boundary conditions on the flow model. Exact solutions are obtained for flow transport, temperature distribution besides that heat transfer rate and friction drag in terms of Mittag-Leffler function by using Fourier sine and Laplace techniques as hybrid methods. Further, we provided the limiting case solutions for classic partial differential equations on obtained governing fluid flow models. The influence of various physical parameters with different fractional orders are investigated on hybrid nanofluid's fractional momentum and energy by plotting velocity and energy curves. Few of the findings suggest that fractional parameters have significant effect on flow parameters and that blade-shaped nanoparticles have a high heat transfer rate. The graphical results reveal that the Grashof number shows a symmetry effect in the case of cooling and heating the plate. Furthermore, the performance of hybrid nanofluid is considerably more effective with the Caputo-fractional derivatives rather than in the classic derivative approach.

Keywords: Casson Fluid; Fourier Sine Transform; Laplace Transform; fractional heat equation; shape factor; Mittag-Leffler function

Citation: Lisha, N.M.; Vijayakumar, A.G. Analytical Investigation of the Heat Transfer Effects of Non-Newtonian Hybrid Nanofluid in MHD Flow Past an Upright Plate Using the Caputo Fractional Order Derivative. *Symmetry* **2023**, *15*, 399. https://doi.org/10.3390/sym15020399

Academic Editors: António Lopes, Alireza Alfi, Liping Chen and Sergio Adriani David

Received: 25 November 2022
Revised: 13 December 2022
Accepted: 19 December 2022
Published: 2 February 2023

1. Introduction

Nanotechnology has significantly advanced in heat transfer studies, which has enhanced the thermal characteristics of energy-transmitting fluids. Producing nanoparticles with great heat conductivity is one of the most trending uses of nanotechnology. To increase the thermal conductivity of fluids, nanofluids have great importance. They are prepared in laboratories by using nanoparticles with an average diameter of less than 100 nm which are suspended in typical heat transfer fluids such as oil, water, and ethylene glycol. First, Maxwell [1] proposed nanofluids after an attempt to optimize the heat transfer rate of regular fluids by suspending micro-sized particles failed owing to sedimentation and clogging of the flow patterns. Based on these issues, Choi [2] suggested in 1995 that the dispersion of nanoparticles into the host fluid might improve the thermal performance of the base fluid. Subsequently, a diverse range of devices have been developed for a variety of practical purposes and functions in various fields such as electrical engineering [3], helping to improve the thermal efficiency of horizontal spiral coils used in solar ponds [4], as a coolant in double pipe heat exchangers [5], stenotic artery [6] and drug agent [7]. Later research by Imran Siddique et al. [8], Maryam Aleem et al. [9], as well as Anum Shafiq et al. [10] broadened the literature on nanofluids. The discovery of nanofluids has achieved the major part of industry's requirements, but the suspension of single nanoparticles is inadequate for the required thermal performance. Therefore, researchers have been attempting to develop a better and more efficient fluid. Yamada et al. [11] defined an upgraded kind of nanofluid in 1989 by combining two or more nanoparticles of distinct characteristics with common fluids. This advanced categorization of nanofluid, known as a hybrid nanofluid, shows potential improvements in heat transfer rate, which can be applied in many domains such as biomedicine [12–14], heat exchangers [15], solar energy [16] and so on. Some of the modern advances in the literature of hybrid nanofluids are observed in the studies carried by Hafeez et al. [17]; their study provides a numerical modelling of MHD rotational flow of hybrid nanomaterial by applying a bvp4c technique between two parallel porous sheets. Iskandar Waini et al. [18] examined the stable mixed convection flow along a vertical surface immersed in a porous medium using hybrid nanoparticles. Talha Anwar et al. [19] established two independent fractional models, Caputo–Fabrizio and Atangana–Baleanu, to analyze the flow patterns and thermal characteristics of a NaAlg/SA-based hybrid nanofluid. Their study revealed that the CF fractional operator improves the thermal rate more efficiently than the AB fractional operator.

Heat transmission is crucial for temperature controls in many industrial applications. Even with increased demand for energy-efficient equipment, achieving good heat transmission of a fluid remains a challenge. As a result, nanoparticles, nanofluids, and hybrid nanofluids exploration are some of the most significant topics of research. Consequently, heat transfer becomes more robust. Nepal T. Balaji et al. [20] investigated the micro channel heat sink, which is used to check the convective heat transfer properties of water-based hybrid nanofluids including graphene nanoplatelets and MWCNTs. Mumtaz Khan et al. [21] examined FDM combined with L1-technique utilization to perform the heat transfer of fractional transient MHD flow of viscoelastic hybrid nanofluids through an inclined surface fixed in a Darcy porous medium. Unsteady natural convection and heat transmission of hybrid nanofluid for two upright parallel plates were analyzed by Chandra Roy and Ioan Pop [22]. In the fields of biomechanics, aerospace, and chemical engineering, magnetohydrodynamics (MHD) free convection flow is extremely important. MHD primarily focuses on the study of the magnetic characteristics and behavior of electrically conducting fluids, including magneto fluids such as electrolytes, liquid metals, plasmas and salt water. Ndolane Sene [23] examined the heat transmission analysis of Brinkmantype fluid with Caputo derivative. Zar Ali Khan et al. [24] found the analytic solution of the transient flow of a generalized Brinkman-type fluid in a channel under the influences of MHD with Caputo–Fabrizio fractional derivative. Ridhwan Reyaz et al. [25] explored the effects of heat radiation on the MHD Casson Fluid as well as the Caputo fractional derivative on an oscillating upright plate.

The investigation of non-Newtonian materials is another intriguing research issue due to its interdisciplinary character and interesting rheological dynamics. Non-Newtonian fluids are flexible due to their applicability in numerous sectors and production processes. The relevance of non-Newtonian fluids may be seen in the oil packing, cooling/heating processes, hydraulics, lubricant industry and opto-electronics. In the literature, scientists have researched many non-Newtonian models, among which is included the Casson Fluid model [26], made known in 1959 by Casson, while inspecting the rheological data of pigment ink in a printer. Casson Fluid is a shear-thinning liquid with infinite viscosity at zero shear stress. When the yield stress is higher than the shear stress, the fluid acts like a solid. Toothpaste, slurries, blood, paint, molten polymers, honey, jelly, tomato sauce and chocolate are examples of Casson Fluid. This fluid model has been beneficial to polymer processing industries, food manufacturers, cosmetics, textiles, biomechanics, pharmaceuticals and many more. Ali Raza et al. [27] investigated the flow of Casson nanoparticles by applying Laplace Transform across a vertical moving plate using the Atangana–Baleanu time-fractional derivative and studies have shown that the fractional, ordinary velocity fields of Casson Fluid decreases when compared to viscous fluid. Muhammad Nazirul Shahrim et al. [28] were using the Laplace Transform to study the precise solution of fractional convective

Casson Fluid over an accelerated plate. M. Veera Krishna et al. [29] explored the radiative MHD flow of Casson hybrid nanofluid through an infinite exponentially accelerated vertical porous surface using the Laplace methodology, and the temperature of Casson hybrid nanofluid is considerably superior to that of Casson nanofluid.

In present times, fractional calculus [30] is essential in engineering and applied scientific disciplines such as physics, electronics, mechanics, population modelling, biosciences, economics and signal processing. Fractional calculus contains two categories singular operators and nonsingular operators. (1) Caputo derivative (2) Riemann–Liouville derivative are singular operators. The Caputo–Fabrizio derivative and the Atangana–Baleanu derivative are non-singular operators. They arose as a result of the application of conventional differentiation to the concept of non-local derivatives. As per several subject specialists, the findings obtained through the use of fractional operators are more precise and realistic than those obtained using classic differentiation. When it comes to understanding fluid performance, fractional operators are extremely important because of their self-similar qualities and memory-capturing capabilities. The Caputo derivative is the most commonly encountered derivative in the fractional calculus literature. The rationale stems from the fact that this derivative is consistent with the initial conditions utilized in modelling real-world issues. Michele Caputo proposed the Caputo fractional derivative in his study in the year 1967 [31]. Talha Anwar et al. [32] analyzed different shape effects of fractal fractional model for thermal analysis of hybrid nanofluid with a power-law kernel and noticed that the heat transfer rate was most effective for blade-shaped nanoparticles when graphene nanoparticles and graphite oxide were equally dispersed. Muhammad Saqib et al. [33] used the Atangana–Baleanu fractional derivative to examine the time fractional model of the convective flow of carboxy–methyl–cellulose (CMC)-based CNTs nanofluid through a porous media in a microchannel and observed that MWCNTs are more efficient than SWCNTs in improving the thermal conductivity of the nanofluids. Marjan Mohd Daud et al. [34] implemented the Caputo fractional derivative principle to Casson Fluid convective flow in a microchannel with radiant heat flux. M Ahmad et al. [35] described a generalization for natural convection flow of Maxwell nanofluid in two upright parallel plates adopting Caputo–Fabrizio utility of fractional order derivatives. Sidra Aman et al. [36] derived precise estimates for MHD flow of Casson nanofluid with hybrid nanoparticles using the Caputo time fractional derivatives.

Being motivated by Ndolane Sene [37], who analyzed the exact solution for a class of fluids model with the Caputo derivative by using Laplace and Fourier Sine Transform method, it is noticed that there has been no attempt in the prior literature to investigate MHD and hybrid nanofluids with Caputo fractional derivatives by using Fourier Sine Transform and Laplace Transform. Hence, the current study proposes to expand on the work of Ndolane Sene by adopting MHD with different shapes of hybrid nano fluid model using graphene (Gr), multiwall carbon nanotubes (MWCNTs) as nanoparticles and water as host fluid to analyze the heat transmission rate. The implementation of the Caputo derivative and its approach to obtaining the analytical results by employing the Laplace and Fourier transforms will be novel. The Caputo fractional derivative is used to fractionalize the MHD free convection Casson hybrid Brinkman-type fluid model. The Fourier sine and Laplace Transformation is used to transform non-linear governing PDEs into ordinary differential equations. These exact solutions are shown for temperature and flow fields of hybrid nanofluid. Eventually, by making $\alpha \to 1$, $\beta \to \infty$ the classic non-Newtonian solutions are recovered for velocity field. Further, the influence of several parameters on the fluid flow and thermal characteristics were discussed and shown in graphical and tabular form. The practical applications of employing these nanoparticles are in wastewater treatment, 3D printing, solar cell (dye-sensitized solar cells) industries.

The contents of the present paper are outlined as follows. Section 2 describes the fractional mathematical model using Caputo fractional derivatives. Section 3 gives the approaches to obtain analytical solutions using Fourier sine and Laplace Transform methods for temperature and velocity fields. Further discussed are the limiting cases, heat transmission rate and shearing stress. Discussion and the interpretations of the influences of the parameters utilized in the modelling have been provided in Section 4. We conclude the paper with findings which are discussed in Section 5.

2. Fractional Mathematical Model with Caputo Derivative

Consider an unsteady MHD free convective Casson hybrid flow of water with graphene and MWCNTs nanoparticles over an infinite upright plate. The system rectilinear coordinate is implemented for the analysis, and the fluid flow is taken in the y-direction, whereas the x-axis is picked perpendicular to the plate. Magnetic field of strength B_0 is applied normal to the fluid flow direction. The fluid is viscous, incompressible, conducting and not electrified. The fluid is assumed to be gray, absorbing and emitting radiation but as a non-scattered medium. Different forms of nanoparticles (cylinder, blade, brick, platelet and spherical) are disseminated into the host fluid to obtain hybrid nanofluid. At time $\tau = 0$, the plate and hybrid nanofluid are both in equilibrium state with temperature T_∞. As time progresses, $\tau > 0$, the fluid is driven by the velocity U and at the same time, temperature of the fluid raised to T_W and then far away from the plate its ambient temperature is T_∞, causing free convection to occur, as presented in Figure 1. Body force emerges as buoyancy force in this circumstance because of the temperature difference. Further, for analyzing the flow phenomena of the hybrid nanofluid, the Brinkman-type fluid model is being used.

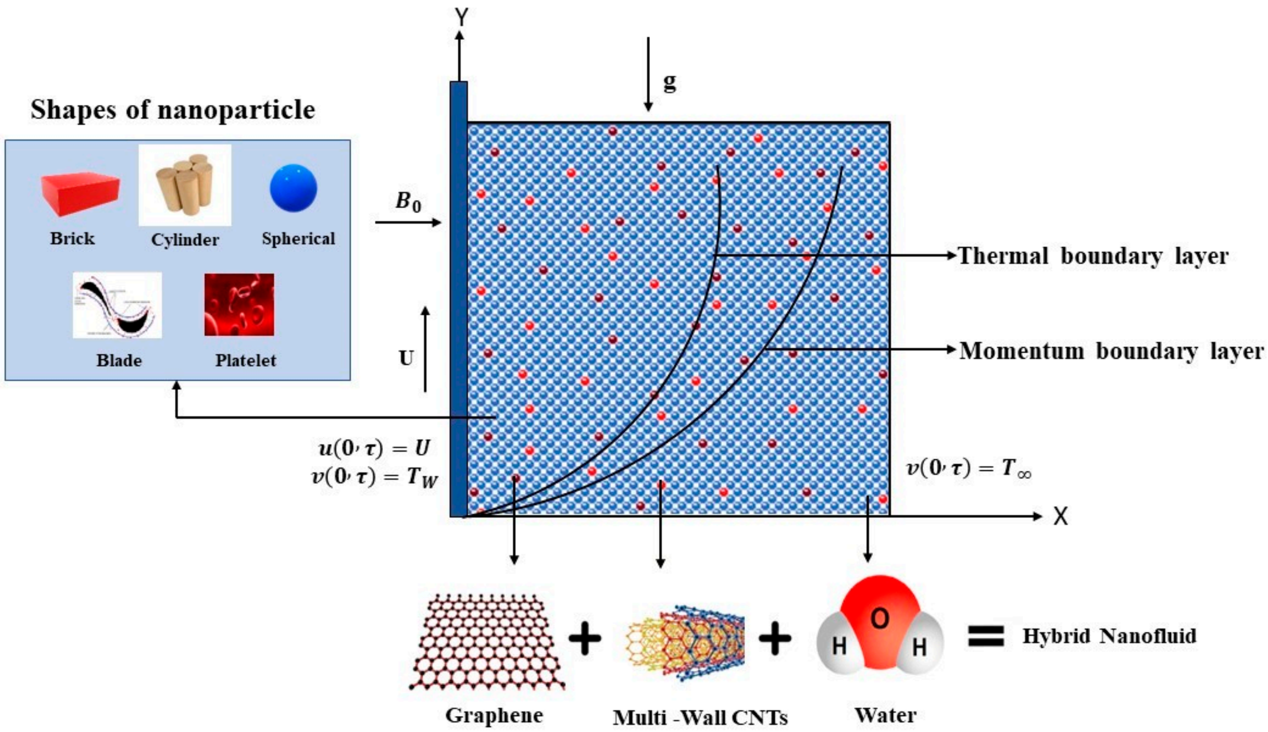

Figure 1. Flow geometry.

The following forms can be used to depict the rheological equation for an incompressible Casson Fluid (Nakamura et al. [38]).

$$\left.\begin{aligned} \pi_{i,j} &= 2(\mu_\gamma + \tfrac{p_y}{\sqrt{2\pi}})e_{ij} \quad when\ \pi > \pi_c \\ \pi_{i,j} &= 2(\mu_\gamma + \tfrac{p_y}{\sqrt{2\pi_c}})e_{ij} \quad when\ \pi < \pi_c \end{aligned}\right\} \tag{1}$$

Here, $\pi = e_{ij}e_{ij}$ where e_{ij} represents the $(i,j)^{th}$ component of the deformation rate, π is the product of the component of deformation rate with itself, π_c is the critical value of this product based on the non-Newtonian model, p_y symbolizes the yields stress, and μ_γ denotes the plastic dynamic viscosity of the non-Newtonian flow.

The mathematical structure of the corresponding conventional flow of Casson hybrid nanofluid (graphene–MWCNTs–H_2O) can be concise by Boussinesq's approximation (Nehad Ali Shah and Ilyas Khan [39]) with the following partial differential governing equations given under the aforementioned assumptions.

$$\frac{\partial u}{\partial x} + \frac{\partial v}{\partial y} = 0 \tag{2}$$

$$\rho_{hnf}\frac{\partial u}{\partial t} = \mu_{hnf}(1+\frac{1}{\beta})\frac{\partial^2 u}{\partial x^2} + \rho_{hnf}\gamma_{hnf}g(T-T_\infty) - \sigma_{hnf}B_0^2 u \tag{3}$$

$$(\rho C_p)_{hnf}\frac{\partial T}{\partial t} = \kappa_{hnf}\frac{\partial^2 T}{\partial x^2} \tag{4}$$

The dimensional initial and boundary conditions employed in this study are detailed below.

$$\begin{array}{ll} t \le 0: & u = 0, T = T_\infty \forall x \\ t > 0: & \begin{array}{c} u = U,\ T = T_w : x = 0 \\ u \to 0,\ T \to T_\infty : x \to \infty \end{array} \end{array} \tag{5}$$

Table 1 lists the thermo-physical attributes of hybrid nanofluids and nanofluids. Table 2 portrays the thermophysical properties of the host fluid (H_2O) and nanoparticles (graphene and MWCNT). Table 3 displays the sphericity and shape factor for various shapes of nanoparticles.

Table 1. Hybrid nanofluid thermophysical description (Talha Anwar et al. [32]).

Properties	Hybrid Nanofluid
Viscosity, μ	$\mu_{hnf} = \frac{\mu_f}{(1-\phi_{Gr})^{2.5}(1-\phi_{MWCNT})^{2.5}}$ (Brinkman model)
Density, ρ	$\rho_{hnf} = \left[\rho_f(1-\phi_1) + \phi_1\rho_{p_1}\right](1-\phi_2) + \rho_{p_2}\phi_2$
Specific heat capacity, C_ρ	$(\rho C_p)_{hnf} = \left[\phi_{Gr}(\rho C_p)_{Gr} + (1-\phi_{Gr})(\rho C_p)_f\right](1-\phi_{MWCNT}) + (\rho C_p)_{MWCNT}\phi_{MWCNT}$
Thermal conductivity, κ	$\kappa_{hnf} = \kappa_{nf}\left[\frac{\kappa_{MWCNT}+(n-1)\kappa_{nf}-(n-1)(\kappa_{nf}-\kappa_{MWCNT})\phi_{MWCNT}}{\kappa_{MWCNT}+(n-1)\kappa_{nf}+(\kappa_{nf}-\kappa_{MWCNT})\phi_{MWCNT}}\right]$ (Maxwell model) where $\kappa_{nf} = \kappa_f\left[\frac{\kappa_{np_1}+\kappa_f(n-1)-(\kappa_f-\kappa_{np_1})(n-1)\phi_{np_1}}{\kappa_{np_1}+\kappa_f(n-1)+(\kappa_f-\kappa_{np_1})\phi_{np_1}}\right]$
Electrical conductivity, σ	$\sigma_{hnf} = \sigma_{nf}\left[\frac{\sigma_{p_2}+(n-1)\sigma_{nf}-(n-1)(\sigma_{nf}-\sigma_{p_2})\phi_2}{\sigma_{p_2}+(n-1)\sigma_{nf}+(\sigma_{nf}-\sigma_{p_2})\phi_2}\right]$ where $\sigma_{nf} = \sigma_f\left[\frac{\sigma_{p_1}+(n-1)\sigma_f-(n-1)(\sigma_f-\sigma_{p_1})\phi_1}{\sigma_{p_1}+(n-1)\sigma_f+(\sigma_f-\sigma_{p_1})\phi_1}\right]$
Thermal expansion coefficient, γ	$(\rho\gamma)_{hnf} = \left[(1-\phi_{Gr})(\rho\gamma)_f + \phi_{Gr}(\rho\gamma)_{Gr}\right](1-\phi_{MWCNT}) + (\rho\gamma)_{MWCNT}\phi_{MWCNT}$

Table 2. Thermophysical characteristics of the host fluid and nanoparticles (Mumtaz Khan et al. [21], Reddy SR and Reddy PB [40]).

Physical Properties	Water (H_2O)	Graphene (Gr)	Multiwall Carbon Nanotube (MWCNT)
ρ/Kgm^{-3}	997.1	2250	1600
$C_\rho/\text{JKg}^{-1}\text{K}^{-1}$	4179	2100	796
$\kappa/\text{Wm}^{-1}\text{K}^{-1}$	0.613	2500	3000
σ/Sm^{-1}	5.5×10^{-6}	10^7	10^7
γ/K^{-1}	210×10^{-6}	-7×10^{-6}	2.1×10^{-5}

The following non-dimensional parameters are constructed using Buckingham's pi-theorem (W.D.Curtis [41]).

Table 3. Sphericity and shape factor of nanoparticles of various shapes (Muhammad Saqib et al. [33]).

Models	**a**	**b**	ψ	$p=\frac{3}{\psi}$
Blade	14.6	123.3	0.36	8.3
Brick	1.9	471.4	0.81	3.7
Platelet	37.1	612.6	0.52	5.7
Cylinder	13.5	909.4	0.62	4.9
Spherical	-	-	1	3

$$\begin{gathered} u^* = \frac{u}{U},\ x^* = x\frac{U}{v},\ \tau^* = \frac{U^2}{v}t,\ v = \frac{T - T_\infty}{T_w - T_\infty} \\ Pr = \frac{(\mu C_p)_f}{\kappa_f},\ Gr = \frac{g v_f \gamma_f (T_w - T_\infty)}{U^3},\ M = \frac{\sigma_f v_f B_0^2}{\rho_f U^2} \end{gathered} \tag{6}$$

When transforming the Equations (2)–(5) using the dimensionless variables specified in Equation (6) and further dropping * sign, a more simplified form of the non-dimensional fluid model is obtained as:

$$\frac{\partial u}{\partial \tau} = a_7(1 + \frac{1}{\beta})\frac{\partial^2 u}{\partial x^2} - a_{10}M + a_{12}Grv \tag{7}$$

$$\frac{\partial v}{\partial \tau} = \frac{a_4}{Pr}\frac{\partial^2 v}{\partial x^2} \tag{8}$$

Fractional calculus is an effective tool for describing real-world phenomena with the so-called memory effect. The Caputo derivative is used because the memory effect and a constant function's derivatives yield zero. Equations (9) and (10) are obtained by replacing the integer order derivative with the Caputo derivative in Equations (7) and (8) and generalizing the integer-order derivative to non-integer partial differential equations. They are:

$$D_\tau^\alpha u = a_7(1 + \frac{1}{\beta})\frac{\partial^2 u}{\partial x^2} - a_{10}M + a_{12}Grv \tag{9}$$

$$D_\tau^\alpha v = \frac{a_4}{Pr}\frac{\partial^2 v}{\partial x^2} \tag{10}$$

We treat the following relationships as dimensional initial and boundary conditions that momentum and temperature satisfy.

$$\begin{array}{ll} \tau \le 0: & u = 0,\ v = 0 \forall x \\ \tau > 0: & \begin{array}{c} u = 1,\ v = 1 : x = 0 \\ u \to 0,\ v \to 0 : x \to \infty \end{array} \end{array} \tag{11}$$

where

$$\begin{gathered} a_1 = \frac{\kappa_{p_2} + (n-1)\kappa_{nf} - (n-1)(\kappa_{nf} - \kappa_{p_2})\phi_2}{\kappa_{p_2} + (n-1)\kappa_{nf} + (\kappa_{nf} - \kappa_{p_2})\phi_2}, \\ a_2 = \frac{k_{p_1} + (n-1)k_f - (n-1)(k_f - k_{p_1})\phi_1}{k_{p_1} + (n-1)k_f - (k_f - k_{p_1})\phi_1}, \\ a_3 = (1 - \phi_2)\left[(1 - \phi_1) + \phi_1 \frac{(\rho C_p)_{p_1}}{(\rho C_p)_f}\right] + \left[\frac{(\rho C_p)_{p_2}}{(\rho C_p)_f}\right]\phi_2, a_4 = \frac{a_1 a_2}{a_3}, \\ a_5 = (1 - \phi_1)^{2.5}(1 - \phi_2)^{2.5}, a_6 = (1 - \phi_2)\left[(1 - \phi_1) + \phi_1 \frac{\rho_{p_1}}{\rho_f}\right] + \left[\frac{\rho_{p_2}}{\rho_f}\right]\phi_2, a_7 = \frac{1}{a_5 a_6}, \\ a_8 = \frac{\sigma_{p_2} + (n-1)\sigma_{nf} - (n-1)(\sigma_{nf} - \sigma_{p_2})\phi_2}{\sigma_{p_2} + (n-1)\sigma_{nf} + (\sigma_{nf} - \sigma_{p_2})\phi_2}, \\ a_9 = \frac{\sigma_{p_1} + (n-1)\sigma_f - (n-1)(\sigma_f - \sigma_{p_1})\phi_1}{\sigma_{p_1} + (n-1)\sigma_f + (\sigma_f - \sigma_{p_1})\phi_1}, \\ a_{10} = \frac{a_8 a_9}{a_6}, a_{11} = (1 - \phi_2)\left[(1 - \phi_1) + \phi_1 \frac{(\rho\gamma)_{p_1}}{(\rho\gamma)_f}\right] + \frac{(\rho\gamma)_{p_2}}{(\rho\gamma)_f}\phi_2,\ a_{12} = \frac{a_{11}}{a_6} \end{gathered}$$

3. Procedure for Solution

There are numerous approaches for solving the fractional differential equations provided in Equations (9) and (10). This section explains how to use analytical approaches to find solutions. In this work, Laplace and Fourier Sine Transformation are used to find exact results for our present model. This approach is mentioned in the following literatures [42,43]. The benefit of this method in this study is that it allows for the development of linear fractional differential equations. Figure 2 shows a flowchart that summarizes the solution method used in this study.

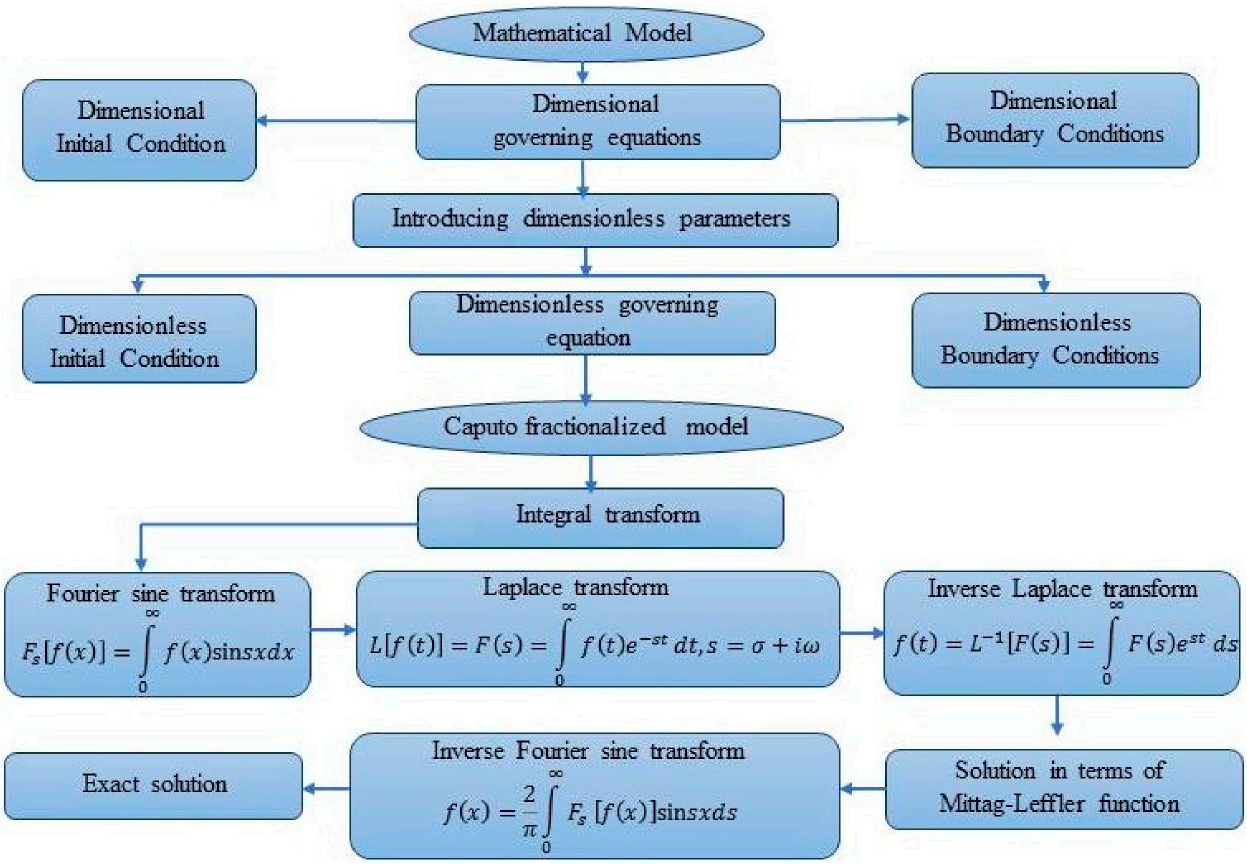

Figure 2. Flow chart for Fourier sine and Laplace Transform.

3.1. Integral Transform for Fractional Order Caputo Derivative

The Laplace Transform method is employed for obtaining accurate analytical solutions in this study, the Laplace Transformation of the Caputo derivative in the following lines are defined.

The Caputo fractional derivative of $f(t)$ is defined as:

$$D^{\alpha} f(t) = \frac{1}{\Gamma 1 - \alpha} \int_0^t (t-s)^{-\alpha} \frac{df(s)}{ds};\ 0 < \alpha < 1 \tag{12}$$

where α is a fractional order, Γ is a gamma Euler function.

In Equation (12), the Laplace Transform and the Convolution theorem is utilized to obtain:

$$L\left[\int_0^t f'(u)(t-u)^{-\alpha} du\right] = \left(s\bar{f}(s) - f(0)\right)\frac{\Gamma 1 - \alpha}{s^{1-\alpha}} \tag{13}$$

Then, using the Laplace Transform definition, the following is obtained:

$$L[D_c{}^{\alpha} f(t)] = s^{\alpha} L[f(t)] - s^{\alpha-1} f(0) \tag{14}$$

According to the present study Equation (15) is written as:

$$L[D_c{}^{\alpha} v(q,\tau)] = s^{\alpha} L[v(q,\tau)] - s^{\alpha-1} v(q,0) \tag{15}$$

The Laplace Transform in Equation (15) will be significant in the current investigation.

3.2. Hybrid Fractional Temperature Field Calculation

For solving the fractional temperature equation in Equation (10), initial and boundary conditions given in Equation (11) have been used.

Fourier Sine Transform is applied to Equation (10) as first step in this approach and the RHS and LHS are obtained as follows:

$$F_s[D_{\tau}^{\alpha} v(x,\tau)] = D_{\tau}^{\alpha} v(q,\tau) \tag{16}$$

$$F_s\left[\frac{\partial^2 v(x,\tau)}{\partial x^2}\right] = qv(0,\tau) - q^2 v(q,\tau) \tag{17}$$

where the Fourier Sine Transformation is denoted by F_s and the Fourier sine variable is q.

By replacing Equations (16) and (17) in the Fourier Sine Transform of Equation (10), the below Equation (18) is obtained,

$$D_{\tau}^{\alpha} v(q,\tau) = \frac{a_4}{Pr}[qv(0,\tau) - q^2 v(q,\tau)] \tag{18}$$

Now proceeding to the second part of the approach, which is to apply the Laplace Transformation to Equation (18) and use Equation (11) to obtain,

$$v(q,s) = \frac{qa_4}{sPr\left(s^{\alpha} + \frac{a_4 q^2}{Pr}\right)} \tag{19}$$

After some rearrangement, the Equation (20) is as below.

$$v(q,s) = \frac{a_4 q}{Pr}\left[\left(\frac{1}{s} - \frac{s^{\alpha-1}}{s^{\alpha} + \frac{a_4 q^2}{Pr}}\right)\frac{Pr}{a_4 q^2}\right] \tag{20}$$

To solve Equation (20), the inverse Laplace Transform is used, which generates the following relationship.

$$v(q,\tau) = \frac{1}{q}\left[1 - L^{-1}\left[\frac{s^{\alpha-1}}{s^{\alpha} + \frac{a_4 q^2}{Pr}}\right]\right] \tag{21}$$

In order to obtain the analytical solution for Equation (21), the Mittag-Leffler function [44] is used. That is:

Let $\alpha > 0,\ \beta \in \mathbb{R}$ and $z \in \mathbb{C}$. The Mittag-Leffler function is defined by the series:

$$E_{\alpha,\beta}(z) = \sum_{k=0}^{\infty} \frac{z^k}{\Gamma\alpha k + \beta} \text{ when } \alpha > 0 \text{ and } \beta > 0, \text{ the series is convergent.} \tag{22}$$

By doing so, $\beta = 1$, $z = -\lambda\tau^{\alpha}$ and $\lambda = \frac{a_4 q^2}{Pr}$ in Equation (22) and compare Equations (21) and (22), which after simplification acquire the following form:

$$E_{\alpha}(-\frac{a_4 q^2}{Pr}\tau^{\alpha}) = L^{-1}\left[\frac{s^{\alpha-1}}{s^{\alpha} + \frac{a_4 q^2}{Pr}}\right] \tag{23}$$

By replacing Equation (23) in Equation (21),

$$v(q,\tau) = \left[1 - E_\alpha\left(-\frac{q^2 a_4}{Pr}\tau^\alpha\right)\right]\frac{1}{q} \tag{24}$$

This technique is completed by employing the inverse Fourier Sine Transformation to Equation (24) and use the fact of integration $\int\limits_0^\infty \frac{\sin qx}{q}dq = \frac{\pi}{2}$, resulting in:

$$v(x,\tau) = \frac{2}{\pi}\int\limits_0^\infty v(q,\tau)\sin qx dq$$

$$v(x,\tau) = 1 - \frac{2}{\pi}\int\limits_0^\infty \frac{\sin qx}{q}E_\alpha(-\frac{a_4 q^2 \tau^\alpha}{Pr})dq \tag{25}$$

3.3. Hybrid Fractional Velocity Field Calculation

For solving the fractional momentum equation, the Fourier Sine Transformation is applied to Equation (9) and considering $\mu = 1 + \frac{1}{\beta}$ the simplified equation is

$$D_\tau^\alpha u(q,\tau) = a_7\mu q u(0,\tau) - a_7\mu q^2 u(q,\tau) - a_{10}Mu(q,\tau) + a_{12}Grv(q,\tau) \tag{26}$$

and utilizing the Laplace Transform to Equation (26) with the use of Equation (11) yields that,

$$s^\alpha u(q,s) = a_7\mu q\frac{1}{s} - a_7\mu q^2 u(q,s) - a_{10}Mu(q,s) + a_{12}Grv(q,s) \tag{27}$$

With further simplifications Equation (27), reduces to:

$$u(q,s) = \frac{\mu q a_7}{s(s^\alpha + \mu q^2 a_7 + a_{10}M)} + \frac{Grqa_4a_{12}}{sPr(s^\alpha + \mu q^2 a_7 + a_{10}M)(s^\alpha + \frac{a_4 q^2}{Pr})} \tag{28}$$

where,

$$a(q,s) = \frac{\mu q a_7}{s(s^\alpha + \mu q^2 a_7 + Ma_{10})},$$
$$b(q,s) = \frac{Grqa_4a_{12}}{sPr(s^\alpha + \mu q^2 a_7 + a_{10}M)(s^\alpha + \frac{a_4 q^2}{Pr})}$$

The inverse of the function $b(q,s)$ is rewritten as below.

$$b(q,s) = \frac{Grqa_4a_{12}}{Pr}\left[\frac{s^{\alpha-(1+\alpha)}}{s^\alpha + \frac{a_4 q^2}{Pr}} - \frac{s^{\alpha-(1+\alpha)}}{s^\alpha + \mu a_7 q^2 + Ma_{10}}\right] \tag{29}$$

$$b(q,s) = \frac{Gra_4a_{12}}{Prq(\mu a_7 - \frac{a_4}{Pr} + \frac{Ma_{10}}{q^2})}\left[\frac{s^{\alpha-(1+\alpha)}}{s^\alpha + \frac{a_4 q^2}{Pr}} - \frac{s^{\alpha-(1+\alpha)}}{s^\alpha + \mu a_7 q^2 + Ma_{10}}\right] \tag{30}$$

The inverse of Laplace Transformation is used to Equation (30) to obtain:

$$b(q,\tau) = \frac{Gra_4a_{12}}{Prq(\mu a_7 - \frac{a_4}{Pr} + \frac{Ma_{10}}{q^2})}\left[L^{-1}\left(\frac{s^{\alpha-\beta}}{s^\alpha + \frac{a_4 q^2}{Pr}}\right) - L^{-1}\left(\frac{s^{\alpha-\beta}}{s^\alpha + \mu a_7 q^2 + Ma_{10}}\right)\right] \tag{31}$$

where $\beta = 1 + \alpha$.

Using the Mittag-Leffler function as described in Equation (22) and further simplifying, it reduces to:

$$\tau^\alpha\left[E_{\alpha,\beta}(-\lambda t^\alpha)\right] = L^{-1}\left(\frac{s^{\alpha-\beta}}{s^\alpha + \lambda}\right) \tag{32}$$

By comparing Equations (31) and (32) and substituting $\lambda = \frac{a_4 q^2}{Pr}$, $\lambda = \mu a_7 q^2 + M a_{10}$ the following form is obtained:

$$b(q,\tau) = \frac{Gr a_4 a_{12} \tau^{\alpha}}{Prq(\mu a_7 - \frac{a_4}{Pr} + \frac{Ma_{10}}{q^2})}\left[E_{\alpha,\beta}(-\frac{q^2 a_4}{Pr}\tau^{\alpha}) - E_{\alpha,\beta}(-\mu q^2 a_7 - Ma_{10})\tau^{\alpha}\right] \tag{33}$$

Using the inverse Fourier Sine Transform formula:

$$b(x,\tau) = \frac{2}{\pi}\int_0^{\infty} b(q,\tau)\sin qx dq$$

$$b(x,\tau) = \frac{2Gr a_4 a_{12}}{\pi Pr}\int_0^{\infty} \frac{\sin qx}{q(\mu a_7 - \frac{a_4}{Pr} + \frac{Ma_{10}}{q^2})}\left[E_{\alpha,\beta}(-\frac{q^2 a_4}{Pr})\tau^{\alpha} - E_{\alpha,\beta}(-\mu q^2 a_7 - Ma_{10})\tau^{\alpha}\right]dq \tag{34}$$

Again, the function $a(q,s)$ is rewritten as:

$$a(q,s) = \frac{\mu a_7}{q(\mu a_7 + \frac{Ma_{10}}{q^2})}\left[\frac{1}{s} - \frac{s^{\alpha-1}}{s^{\alpha} + \mu q^2 a_7 + Ma_{10}}\right]$$

and employing the inverse Laplace Transformation, solution is written in terms of Mittag-Leffler function as follows:

$$a(q,\tau) = \frac{\mu a_7}{q(\mu a_7 + \frac{Ma_{10}}{q^2})}\left[1 - L^{-1}\left[\frac{s^{a-1}}{s^{\alpha} + \mu q^2 a_7 + Ma_{10}}\right]\right] \tag{35}$$

$$E_{\alpha,1}(-\lambda\tau^{\alpha}) = L^{-1}\left[\frac{s^{a-1}}{s^{\alpha} + \lambda}\right] \tag{36}$$

Using the inverse Fourier Sine Transform, it implies that,

$$a(q,\tau) = \frac{\mu a_7}{q(\mu a_7 + \frac{Ma_{10}}{q^2})}\left[1 - E_{\alpha}(-q^2\mu a_7 - Ma_{10})\tau^{\alpha}\right]$$

where $\lambda = \mu a_7 q^2 + Ma_{10}$

$$a(x,\tau) = \frac{2}{\pi}\left[\int_0^{\infty} \frac{\mu a_7 \sin qx}{q(\mu a_7 + \frac{Ma_{10}}{q^2})}dq - \int_0^{\infty} \frac{\mu a_7 \sin qx}{q(\mu a_7 + \frac{Ma_{10}}{q^2})}E_{\alpha}(-q^2\mu a_7 - Ma_{10})\tau^{\alpha}dq\right] \tag{37}$$

The exact solution is,

$$u(x,\tau) = a(x,\tau) + b(x,\tau) \tag{38}$$

where,

$$a(x,\tau) = \frac{2}{\pi}\left[\int_0^{\infty} \frac{\mu a_7 \sin qx}{q(\mu a_7 + \frac{Ma_{10}}{q^2})}dq - \int_0^{\infty} \frac{\mu a_7 \sin qx}{q(\mu a_7 + \frac{Ma_{10}}{q^2})}E_{\alpha}(-q^2\mu a_7 - Ma_{10})\tau^{\alpha}dq\right]$$

$$b(x,\tau) = \frac{2Gr a_4 a_{12}}{\pi Pr}\int_0^{\infty} \frac{\sin qx}{q(\mu a_7 - \frac{a_4}{Pr} + \frac{Ma_{10}}{q^2})}\left[E_{\alpha,\beta}(-\frac{q^2 a_4}{Pr})\tau^{\alpha} - E_{\alpha,\beta}(-\mu q^2 a_7 - Ma_{10})\tau^{\alpha}\right]dq$$

3.4. Limiting Cases

3.4.1. Temperature Field for Classic Case with Hybrid Nanoparticles

The temperature expression corresponding to $\alpha \rightarrow 1$ in Equation (10) reduces to the following expression,

$$v(x,\tau) = erfc(\frac{x\sqrt{Pr}}{2\sqrt{\tau a_4}})$$

where $erfc$ is a Gaussian error function.

3.4.2. Velocity Field for Classical Case with Hybrid Nanoparticles

The velocity expression corresponding to $\alpha \rightarrow 1$ in Equation (9) reduces to the following expression.

$$\begin{aligned}
u(x,\tau) &= \tfrac{1}{2}\left[e^{x\sqrt{a_{15}}}erfc\left(\tfrac{x}{2\sqrt{a_7\tau B}} + \sqrt{a_{15}a_7\tau B}\right) + e^{-x\sqrt{a_{15}}}erfc\left(\tfrac{x}{2\sqrt{a_7\tau B}} - \sqrt{a_{15}a_7\tau B}\right)\right] \\
&+ \tfrac{a_{13}}{2a_{14}}\left[e^{x\sqrt{a_{15}}}erfc\left(\tfrac{x}{2\sqrt{a_7\tau B}} + \sqrt{a_{15}a_7\tau B}\right) + e^{-x\sqrt{a_{15}}}erfc\left(\tfrac{x}{2\sqrt{a_7\tau B}} - \sqrt{a_{15}a_7\tau B}\right)\right] \\
&- \tfrac{a_{13}e^{\sqrt{a_{14}}\tau}}{2a_{14}}\left[e^{x\sqrt{a_{16}}}erfc\left(\tfrac{x}{2\sqrt{a_7\tau B}} + \sqrt{a_{16}a_7\tau B}\right) + e^{-x\sqrt{a_{16}}}erfc\left(\tfrac{x}{2\sqrt{a_7\tau B}} - \sqrt{a_{16}a_7\tau B}\right)\right] \\
&- \tfrac{a_{13}}{a_{14}}erfc(\tfrac{x\sqrt{Pr}}{2\sqrt{\tau a_4}}) \\
&+ \tfrac{a_{13}e^{\sqrt{a_{14}}\tau}}{2a_{14}}\left[e^{x\sqrt{\frac{a_{14}Pr}{a_4}}}erfc\left(\tfrac{x\sqrt{Pr}}{2\sqrt{a_4\tau}} + \sqrt{a_{14}\tau}\right) + e^{-x\sqrt{\frac{a_{14}Pr}{a_4}}}erfc\left(\tfrac{x\sqrt{Pr}}{2\sqrt{a_4\tau}} - \sqrt{a_{14}\tau}\right)\right]
\end{aligned}$$

where,

$$B = 1 + \frac{1}{\beta},\ a_{13} = -\frac{Gra_4a_{12}}{Pra_7B - a_4},\ a_{14} = \frac{Ma_4a_{10}}{a_7BPr - a_4},\ a_{15} = \frac{Ma_{10}}{a_7B}, a_{16} = \frac{a_{14}}{a_7B} + \frac{Ma_{10}}{a_7B}$$

3.4.3. Velocity Field for Classic Newtonian Fluid with Hybrid Nanoparticles

In the case of velocity for classical Newtonian fluid, the following expression is obtained by making $\beta \rightarrow \infty$, $\alpha \rightarrow 1$ in Equation (9):

$$\begin{aligned}
u(x,\tau) &= \tfrac{1}{2}\left[e^{x\sqrt{a_{19}}}erfc\left(\tfrac{x}{2\sqrt{a_7\tau}} + \sqrt{a_{19}a_7\tau}\right) + e^{-x\sqrt{a_{19}}}erfc\left(\tfrac{x}{2\sqrt{a_7\tau}} - \sqrt{a_{19}a_7\tau}\right)\right] \\
&+ \tfrac{a_{18}}{2a_{17}}\left[e^{x\sqrt{a_{19}}}erfc\left(\tfrac{x}{2\sqrt{a_7\tau}} + \sqrt{a_{19}a_7\tau}\right) + e^{-x\sqrt{a_{19}}}erfc\left(\tfrac{x}{2\sqrt{a_7\tau}} - \sqrt{a_{19}a_7\tau}\right)\right] \\
&- \tfrac{a_{18}e^{\tau a_{17}}}{2a_{17}}\left[e^{x\sqrt{a_{20}}}erfc\left(\tfrac{x}{2\sqrt{a_7\tau}} + \sqrt{a_{20}a_7\tau}\right) + e^{-x\sqrt{a_{20}}}erfc\left(\tfrac{x}{2\sqrt{a_7\tau}} - \sqrt{a_{20}a_7\tau}\right)\right] \\
&- \tfrac{a_{18}}{a_{17}}erfc(\tfrac{x\sqrt{Pr}}{2\sqrt{\tau a_4}}) \\
&+ \tfrac{a_{18}e^{\sqrt{a_{17}}\tau}}{2a_{17}}\left[e^{x\sqrt{\frac{a_{17}Pr}{a_4}}}erfc\left(\tfrac{x\sqrt{Pr}}{2\sqrt{a_4\tau}} + \sqrt{a_{17}\tau}\right) + e^{-x\sqrt{\frac{a_{17}Pr}{a_4}}}erfc\left(\tfrac{x\sqrt{Pr}}{2\sqrt{a_4\tau}} - \sqrt{a_{17}\tau}\right)\right]
\end{aligned}$$

where,

$$a_{17} = \frac{Ma_4a_{10}}{a_7Pr - a_4},\ a_{18} = -\frac{Gra_4a_{12}}{a_7Pr - a_4},\ a_{19} = \frac{Ma_{10}}{a_7},\ a_{20} = \frac{a_{17}}{a_7} + \frac{Ma_{10}}{a_7}$$

3.5. Analytical Expressions for the Heat Transfer and Shear Stress

Heat transmission rate along with shear stress are two important physical quantities that are analyzed to gain access to a wide range of information, such as efficacy of hybrid nanofluids, elements that improve or deteriorate hybrid nanofluid thermal efficiency, the role of accompanying development in deriving hybrid nanofluid flow patterns, and various others. Utilizing the importance of these values, the following mathematical relationships are predicted, which are mentioned as skin friction coefficient (C_f) and Nusselt number (Nu).

Nusselt number from Equation (25), an analytical expression of the dimensionless rate of heat transfer (Nu) is:

$$Nu = -\frac{\partial v}{\partial x}|_{x=0} = -L^{-1}\left[\lim_{x\to 0}\frac{\partial \overline{v}}{\partial x}\right]$$

$$Nu = \sqrt{\frac{Pr}{a_4}}\frac{\tau^{-\frac{\alpha}{2}}}{\Gamma 1-\frac{\alpha}{2}}$$

Skin friction from Equation (38), an analytical expression of the dimensionless skin friction is given by:

$$C_f = -\frac{\partial u}{\partial x}|_{x=0} = -L^{-1}\left[\lim_{x\to 0}\frac{\partial \overline{u}}{\partial x}\right]$$

$$\begin{aligned} C_f = \quad & \frac{1}{\sqrt{Aa_7}}\left[\frac{t^{-\frac{\alpha}{2}}}{\Gamma-\frac{\alpha}{2}+1} - \sum_{k=1}^{\infty}\frac{(2k-2)!(-1)^k {A_1}^k t^{\alpha(k-\frac{1}{2})}}{2^{2k-1}(k)!(k-1)!\Gamma\alpha(k-\frac{1}{2})+1}\right] \\ & -\frac{A_4}{\sqrt{Aa_7}}\left[\frac{1}{\Gamma-\frac{\alpha}{2}+1}\int_0^t u^{\alpha-1}E_{\alpha,\alpha}(A_3u^{\alpha})(t-u)^{-\frac{\alpha}{2}}du\right] \\ & -\frac{A_4}{\sqrt{Aa_7}}\left[\sum_{k=1}^{\infty}\frac{(2k-2)!(-1)^k {A_1}^k}{2^{2k-1}(k)!(k-1)!\Gamma\alpha(k-\frac{1}{2})+1}\int_0^t u^{\alpha-1}E_{\alpha,\alpha}(A_3u^{\alpha})(t-u)^{\alpha(k-\frac{1}{2})}du\right] \\ & +\frac{A_4}{\sqrt{Aa_7}}\sqrt{\frac{Pr}{a_4}}\left[\frac{1}{\Gamma-\frac{\alpha}{2}+1}\int_0^t u^{\alpha-1}E_{\alpha,\alpha}(A_3u^{\alpha})(t-u)^{-\frac{\alpha}{2}}du\right] \end{aligned}$$

where,

$$A_1 = Ma_{10},\ A_2 = BPra_7,\ A_3 = \frac{A_1a_4}{A_2-a_4},\ A_4 = -\frac{Gra_4a_{12}}{A_1-a_4}$$

4. Graphical Findings and Outcomes

This section goes through graphical examination of temperature, flow field domains obtained for fractional order PDEs and flow parameters appearing in the problem. The fractional fluid model is determined analytically using the Laplace and Fourier Sine Transform methods. The Prandtl number, time, thermal Grashof number, Casson parameter, magnetic field, volume fraction parameters ϕ_1 and ϕ_2 are investigated and justified with a physical perspective. Recognizing the significance of shape effects, nanoparticles are thought to have five distinct shapes (brick, blade, cylinder, spherical and platelet). The impact of various flow characteristics is examined by using plotted curves in Figures 3–20 to illustrate various impacts on flow field, temperature, heat flow rate and friction drag, also illustrated with tables, bar graphs to analyze different elements of the topic under study. These graphical, tabular representations aid in understanding the effects of additional processes such as heat flow and energy fields. This section also includes a pictorial comparison of fractional and classical model-based solutions to emphasize their importance. A complete tabular analysis is also used to analyze the Nusselt number and skin friction.

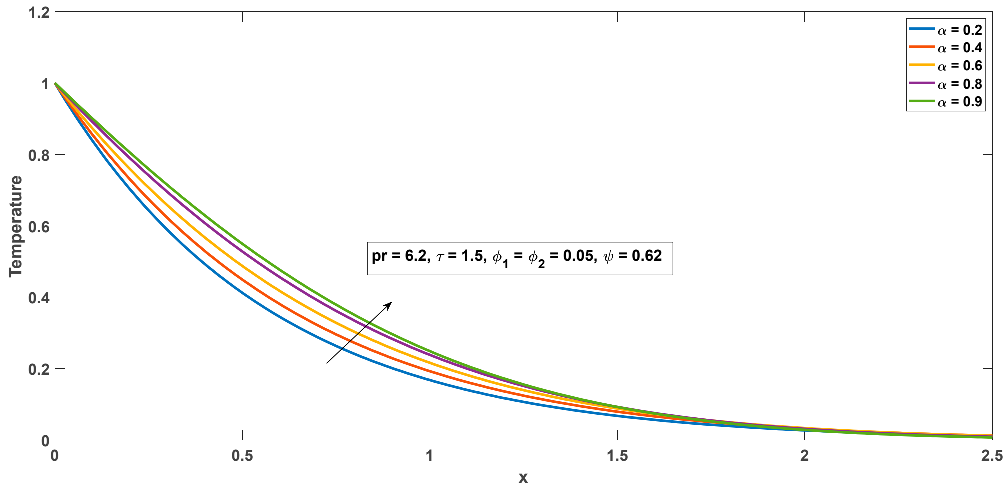

Figure 3. Fluid temperature for varied values of order α.

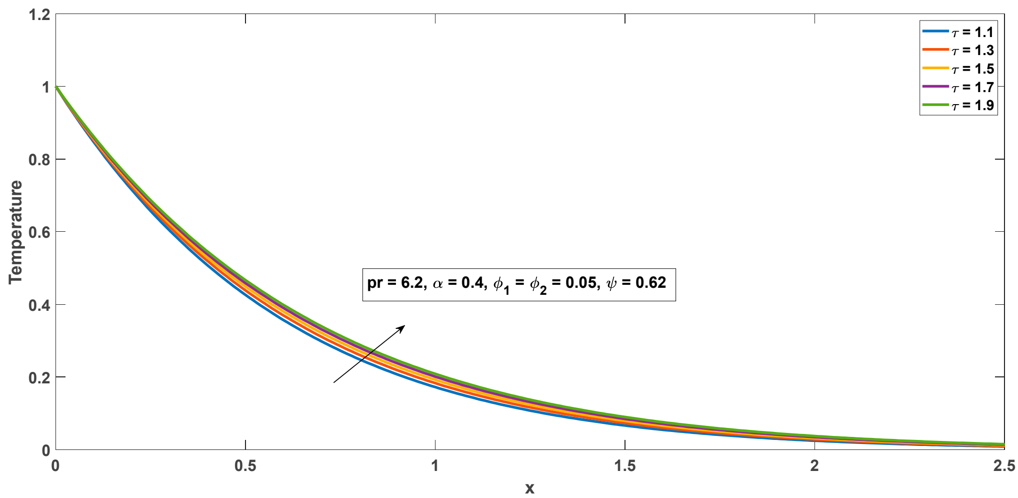

Figure 4. Fluid temperature for varied values of τ.

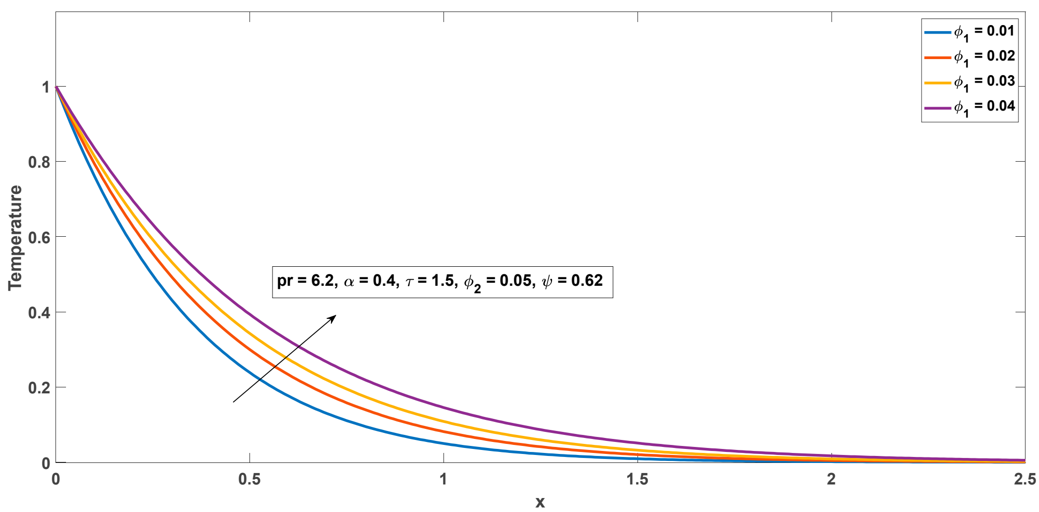

Figure 5. Fluid temperature for varied values of ϕ_1.

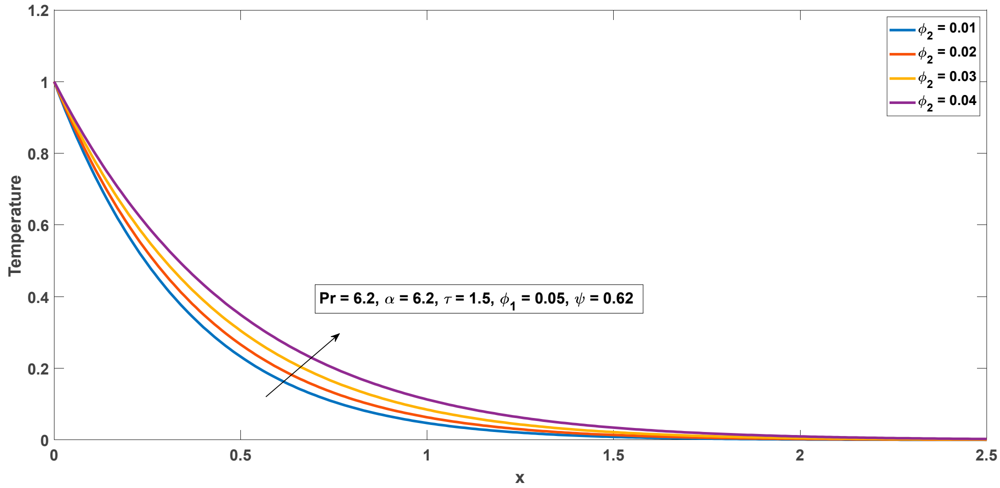

Figure 6. Fluid temperature for varied values of ϕ_2.

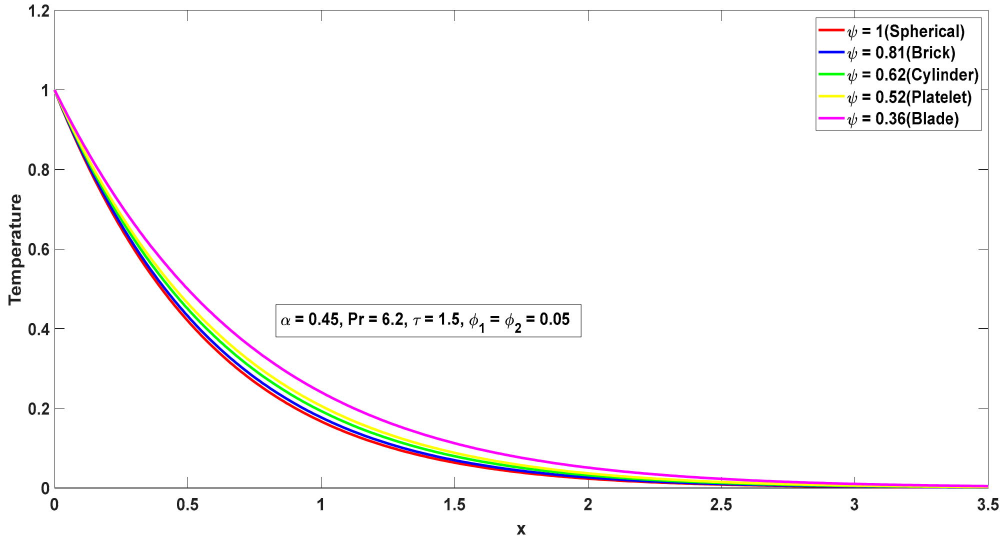

Figure 7. Fluid temperature for distinct shapes.

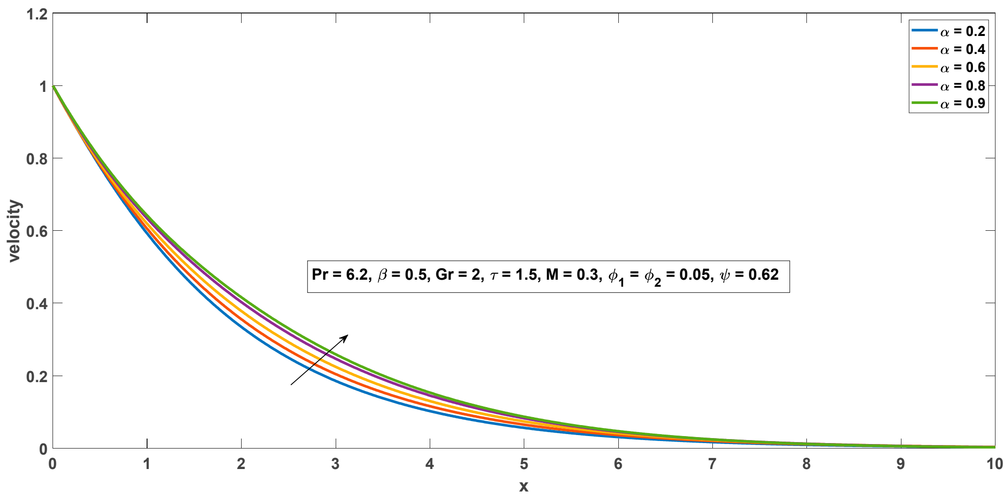

Figure 8. Fluid flow curve for varied values of fractional order α.

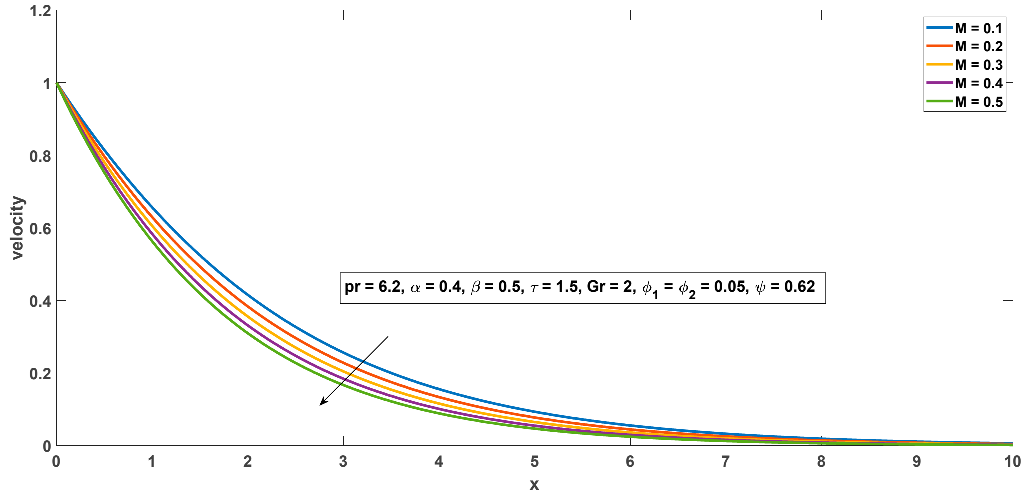

Figure 9. Fluid flow curve for varied values of M.

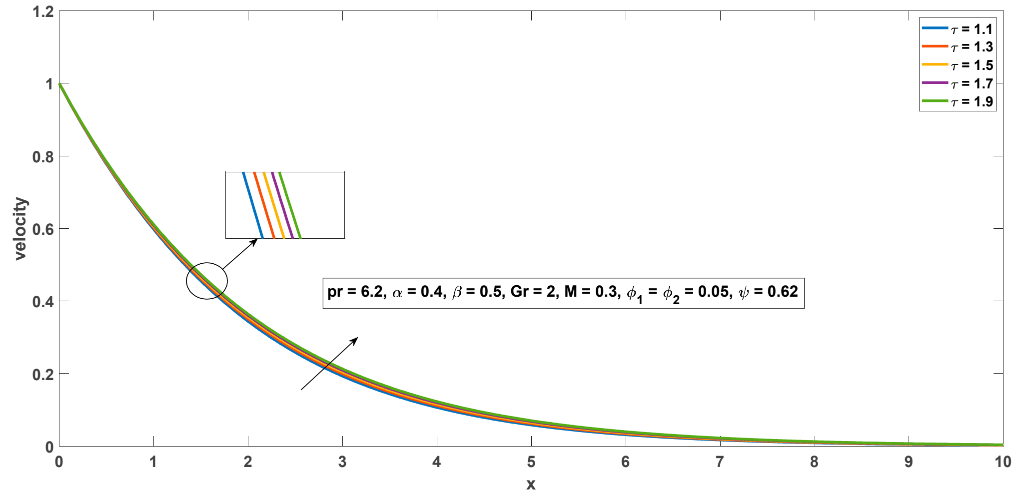

Figure 10. Fluid flow curve for varied values of τ.

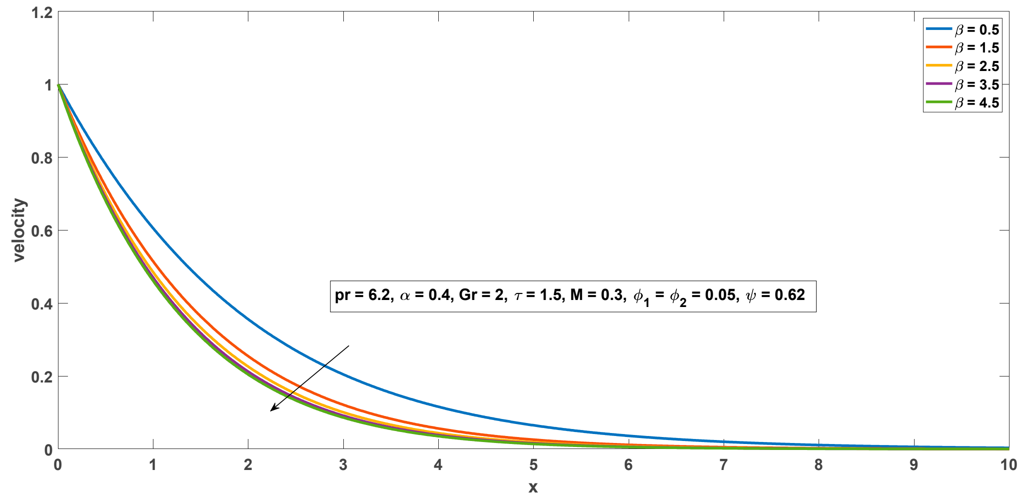

Figure 11. Fluid flow curve for varied values of β.

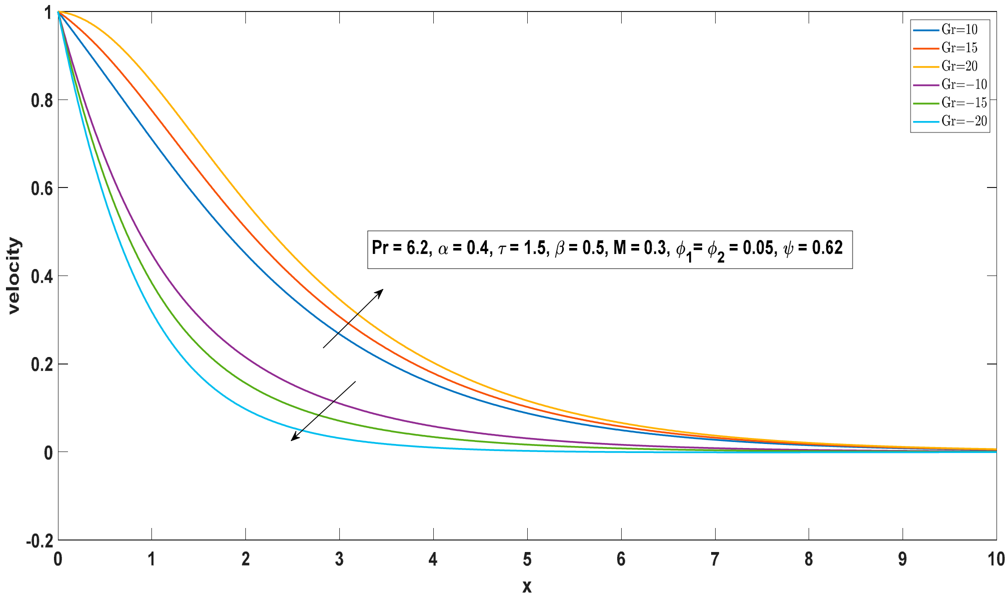

Figure 12. Fluid flow curve for varied values of Gr.

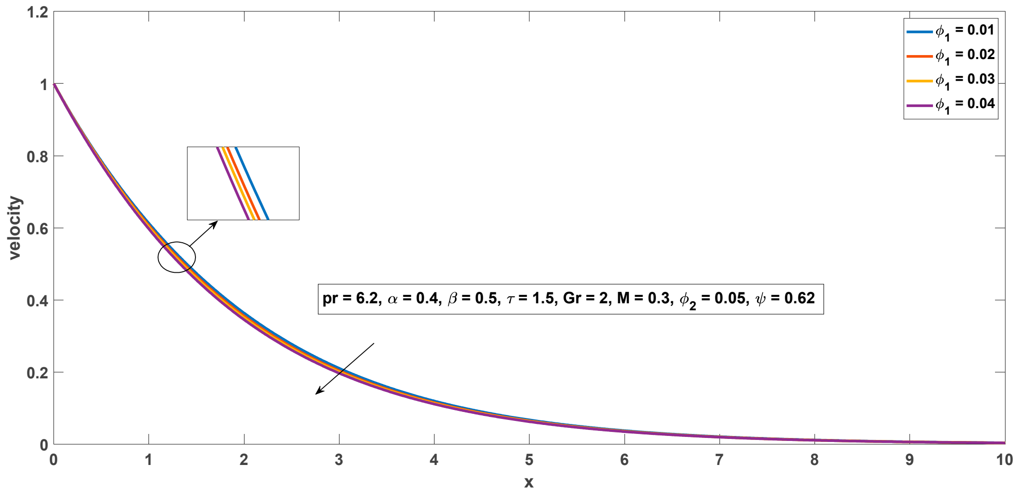

Figure 13. Fluid flow curve for varied values of ϕ_1.

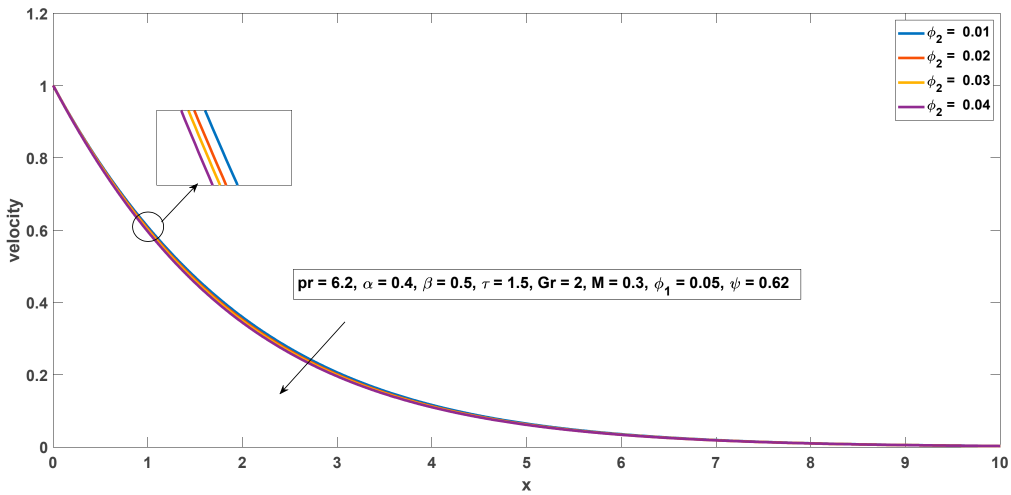

Figure 14. Fluid flow curve for varied values of ϕ_2.

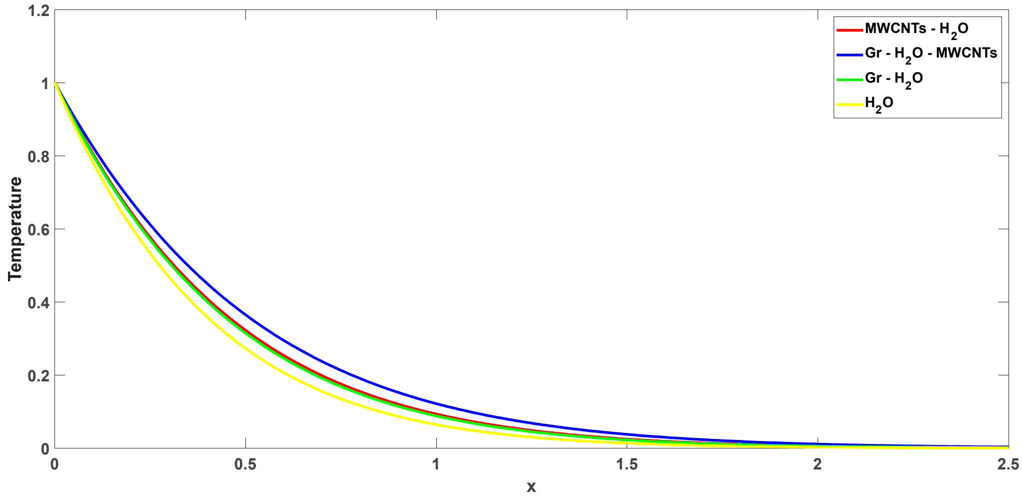

Figure 15. Fluid temperature for distinct nanofluids.

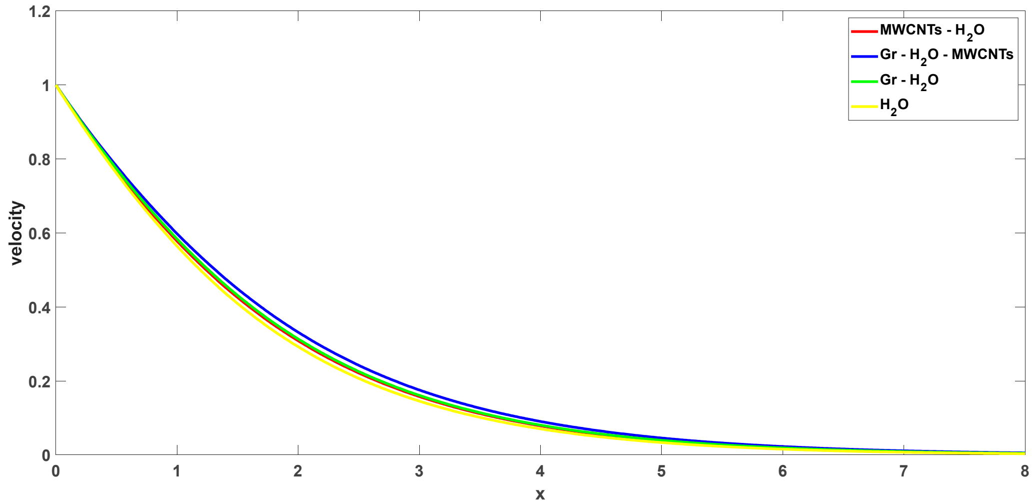

Figure 16. Fluid flow curve for distinct nanofluids.

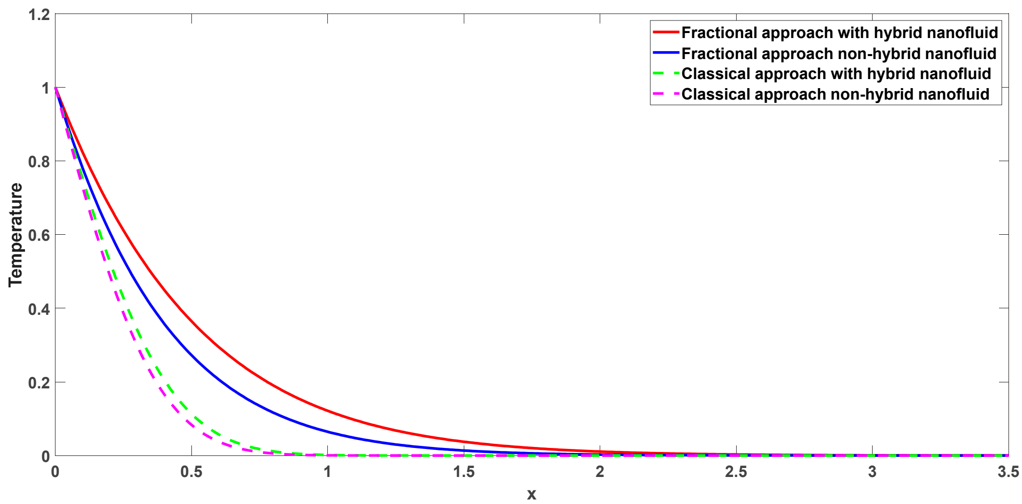

Figure 17. Fluid temperature for different fractional and classical approach.

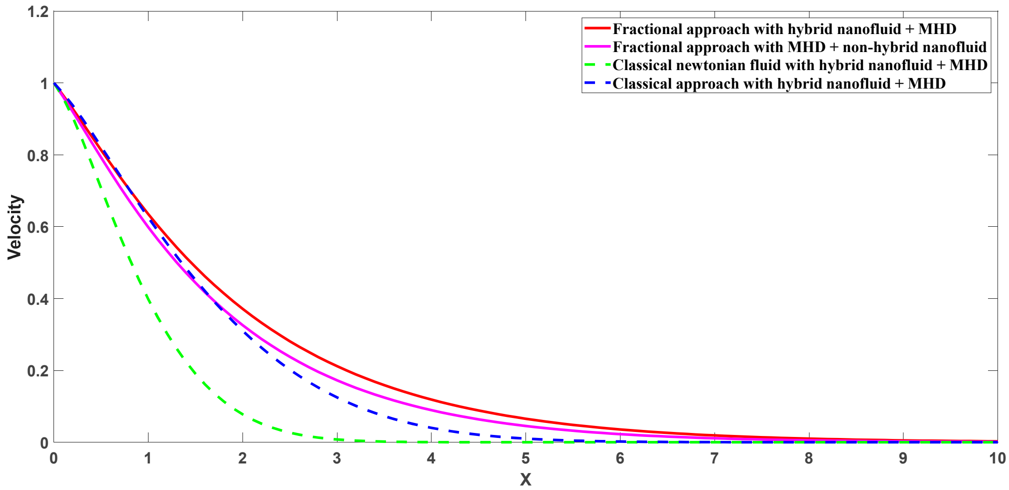

Figure 18. Fluid flow curve for different fractional and non-Newtonian approach.

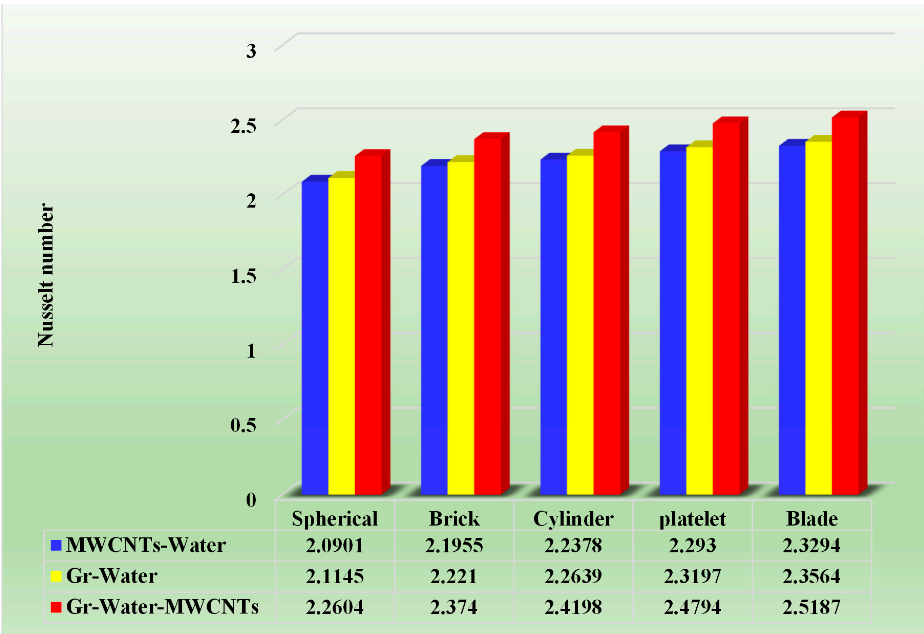

Figure 19. Heat transfer enhancement in different nano particle shape.

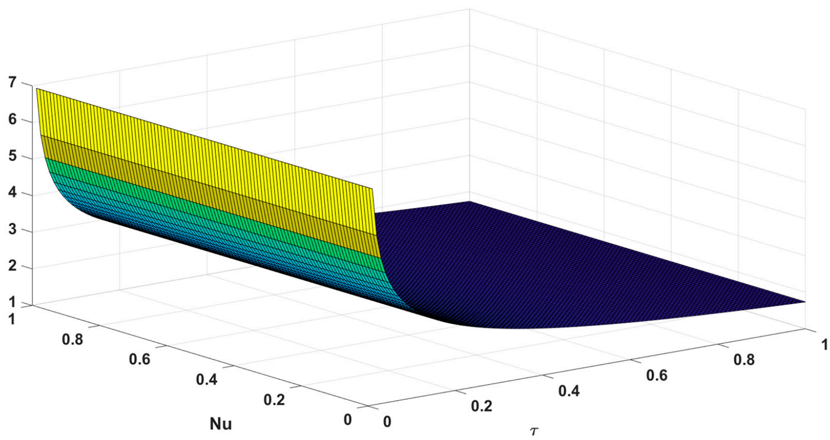

Figure 20. 3D graph for Nusselt number.

4.1. Impact of Physical Parameters on Temperature Field

The energy of Equation (11), whose solution is obtained as presented in Equation (25), has been used for the figures in this section. The temperature profile for fractional order, $\alpha = 0.4$ is considered for various flow parameters.

The impact of fractional parameters against temperature distribution is seen in Figure 3. When $\tau = 1.5$, the temperature field rises with a growing α. Physically, this is explained by the fact that as α increases, the thickness of the thermal boundary layer also increases, which becomes thickest as α approaches 1. The novelty arises from explaining how temperature rises as the order of the fractional operator advances. Because of the memory effect inherent in fractional operators, increases in order have a considerable impact on time value, resulting in a large accumulation. When the order of the fractional operator is raised, it is seen that an increase in time causes a rise in fluid temperature. A sub-diffusion in the range of (0, 1) is also noticed. When the order is modified, the literature's results corroborate Caputo's fractional derivative sub-diffusion (0, 1).

Figure 4 represents the impact of time on the temperature field. In the above fractional case, the temperature rises gradually as the value of time increases. This suggests that when the time under consideration exceeds one, the Caputo derivative has a slower impact on the diffusion process.

The temperature field is considerably impacted by the volume fraction of the hybrid nanofluid, as seen in Figures 5 and 6. The temperature field is noted to grow with increasing volume fraction values, i.e., ϕ_1 and ϕ_2. The physical factors of the hybrid nanofluid clearly show that a rise in ϕ_1 and ϕ_2 leads to an increase in the heat transfer of the hybrid nanofluid, thus resulting in the increase of temperature profile. This is due to the fact that when density of nanoparticles is enhanced, heat conductivity is improved.

The temperature field for different shapes of nanoparticles is represented in Figure 7. Due to the shape factor p included in Table 3, it is seen that the temperature of the blade-shaped nanoparticle is the highest, preceded by the platelet, cylinder, brick, and spherical. It is critical to remember that viscosity decreases as temperature rises. It is obvious that the shapes of platelets, cylinders, and bricks have more viscosity, resulting in lower temperatures, whereas blades and spherical ones have the greatest temperature due to the lowest viscosity. The figure also shows that the spherical form of the nanoparticle has a low viscosity. This is due to the temperature-dependent shear thinning behavior.

4.2. Impact of Physical Parameters on Flow Field

In this section Equation (10), whose solution is obtained as shown in Equation (39) has been taken into account to plot all the figures. Velocity dynamics for distinct flow parameters is illustrated for fractional order situation, $\alpha = 0.4$.

Figure 8 exhibits the impact of fractional order in relation to time. The velocity falls as the order of the Caputo derivative rises. Meaning to say, as order α accelerates the velocity decreases to zero, which also means increasing time causes an increase in the flow field, thus resulting in this outcome.

Figure 9 demonstrates the velocity curve of the magnetic field M parameter. The graph shows that as the magnetic field levels increased, the velocity decreased. This resulted from the application of the transverse magnetic field, which produces the resistive Lorentz force. The Lorentz force, which tends to oppose the flow of hybrid nanofluid, causes the velocity to decrease. When M is raised, the Lorentz force becomes more intense, enabling the hybrid nanofluid to gently come to a halt.

Figure 10 captures the time τ effect on the velocity field, the velocity increases gradually with time growth. This demonstrates that the Caputo derivative has a lesser influence on the diffusion process when the time under consideration reaches one.

Figure 11 shows the consequences of the Casson parameter when the other values are held constant. It illustrates that higher values of β tend to a reduction in fluid velocity. This is due to the physical impact of β, where a larger value of β will increase viscous forces while decreasing thermal forces. Thus, fluid velocity will tend to decrease.

Figure 12 represents the impact of the thermal Grashof number in cooling and heating scenarios. The Grashof number is defined as the ratio of buoyancy force to viscous force acting on a fluid, with fluid motion being linearly dependent on buoyancy force. In convection problems, the thermal Grashof number is responsible for heat transmission. This graph shows how the velocity field rises as the Grashof number increases in case of cooling of the plate $(Gr > 0)$ and the symmetry phenomenon is noted in the heating scenario $(Gr < 0)$. In addition, the symmetry effect is observed from the figure. The Grashof number represents the buoyancy force proportional strength to viscous force; hence, increase in Grashof number corresponds to increase in thermal buoyancy force. As a result, the velocity field tends to expand.

Figures 13 and 14 indicate the effect of hybrid nanofluid volume fraction on flow field. It is noted that the flow field of the hybrid nanofluid decelerates as the values of either ϕ_1 or ϕ_2 increases. The physical explanation for this phenomenon is that as the volume fraction ϕ_1 and ϕ_2 of the hybrid nanoparticle increases, fluid becomes more viscous, resulting in decrement of the nanofluid's flow field. Adding nanomaterials to a fluid raises its density, which decreases both boundary layer thickness and nanofluid velocity; velocity decelerates as time exceeds.

Figures 15 and 16 describe the comparison between the flow field and temperature distribution of the graphene–H_2O–MWCNT hybrid nanofluid to those of the equivalent nanofluids graphene–H_2O and MWCNT–H_2O and the base fluid H_2O. The profiles of the afore stated nanofluids are displayed by employing either $\phi_{Gr} = 0$ or $\phi_{MWCNT} = 0$ in the solutions obtained for hybrid nanofluids. Temperature has been found to be the highest for graphene–H_2O–MWCNT hybrid nanofluid, further observing the trend in temperature profiles followed by MWCNT–H_2O nanofluid, graphene–H_2O nanofluid and base fluid H_2O, in that order. MWCNT nanoparticles have a considerably superior heat-conduction capacity than graphene nanoparticles and water. When MWCNT nanoparticles are disseminated in the host fluid, the resulting MWCNTs–H_2O nanofluid has a higher temperature than graphene–H_2O nanofluid temperature, due to improved thermal and physical features such as heat capacitance and thermal conductivity. Moreover, the even dispersion of considered nanoparticles ($\phi_{Gr} = 0.05 = \phi_{MWCNT}$) improves the thermal conductivity of H_2O in such a way that the heat transfer capacity of the resulting hybrid nanofluid exceeds the heat transfer capacity of H_2O, graphene–H_2O nanofluid and MWCNT–H_2O nanofluid. The performance of the temperature curve is mostly determined by the thermal properties and volume percentage of the nanoparticles under consideration. This temperature fluctuation caused by various nanoparticles emphasizes the importance of nanofluids and hybrid nanofluids in heat control systems. Moreover, H_2O has the higher fluid flow velocity in comparison to other nanoparticles, which is followed by MWCNT–H_2O, graphene–H_2O and H_2O–graphene–MWCNT. The primary cause of these flow patterns is the disparity in nanoparticle density. According to Table 2, the density of host fluid is substantially lower than that of nanoparticles, making it less viscid for everyone. Greater the density of nanoparticles, the more viscid the resulting nanofluid. According to the figure, evenly spreading both nanoparticles in host fluid, results in an increase in the density of hybrid nanofluid.

In Figures 17 and 18, the curves are plotted in order to reveal a comparison between fractional and classical derivative calculus for both cases of hybrid and non-hybrid nanofluids. In the case of temperature, the figure reveals that the temperature of fractional hybrid nanofluid is faster followed by fractional non-hybrid than regular fluids. The fractional derivative model with hybrid nanofluid reveals a better heat transfer enhancement than the classical approach. In the velocity case the fractional hybrid fluid shows the high velocity followed by fractional non- hybrid, Newtonian fluid $(\alpha \to 1,\ \beta \to \infty)$ with hybrid while it has lower velocity for the classical fluid in limiting case.

Figure 19 was plotted to determine the applicability of fractional models for attaining a quicker temperature reduction. In the bar graph shown, numerical values of heat transmission rate (Nu) for fractional derivatives are in comparison with nanofluids and hybrid nanofluids. Moreover, notable emphasis is given to the shape constituent, which resembles certain shapes of disseminated nanoparticles. Heat transmission from vertical plate to hybrid nanofluid happens faster when graphene and MWCNT nanoparticles have a blade form. When spherical-shaped nanoparticles are disseminated in water, the cooling rate of the plate is slower. This disparity in numerical results of Nusselt's number emphasizes the significance of the shape component. Based on these arguments, it is possible to conclude that the morphologies of nanoparticles play a critical part in improving the poor thermal properties of conventional fluids. As a result, evaluating shape factor qualities is an important aspect of such investigations.

The plotting shown in Figure 20 represents the 3D curves for the Nusselt number.

The impact of flow parameters on the Nusselt number is presented in Table 4. According to the table, increasing fractional parameter α, time τ, ϕ_{MWCNT} and ϕ_{Gr} leads to an decrement in the heat transfer rate, whereas increasing Prandtl number Pr, results in heat transfer increasing. The Nusselt number is defined as the ratio of convective heat transfer coefficient to fluid conduction heat transfer; a high Nusselt number value will almost certainly raise the fluid's temperature as heat is transferred at a faster pace, as seen in Figures 3–6.

Table 4. The influence of the various parameters on the Nusselt Number.

ϕ_{Gr}	ϕ_{MWCNT}	Pr	α	τ	Nu
0.02	0.02	6.2	0.6	1.5	1.591572294587753
0.03	-	-	-	-	1.569480227825062
0.04	-	-	-	-	1.547886513587993
-	0.03	-	-	-	1.562898376223181
-	0.04	-	-	-	1.534893820304120
-	-	8	-	-	1.807904639541740
-	-	9	-	-	1.917572445537878
-	-	-	0.8	-	1.332170104172774
-	-	-	0.9	-	1.202904460764115
-	-	-	-	1.7	1.532918522253240
-	-	-	-	1.8	1.506856850036236

Table 5 demonstrates the percent improvement in Nusselt number vs. different volume fraction values of ϕ_{Gr} and ϕ_{MWCNT}. The heat transmission rate of water-based hybrid nanofluid is shown in table for graphene and MWCNT utilized in this investigation, because they have a high heat transfer rate in the base fluid water. It is remarkable that for graphene and multiwall carbon nanotubes in water, the heat flow rate increases by 17.7 percent. This increase in heat transfer rate indicates that radiators used in engines or machines for cooling might be useful for mechanical engineers. Graphene and MWCNT are used as a photoanode and counter electrode in industries for manufacturing solar cells (dye-sensitized solar cells) to increase the efficiency.

Table 6 compares the heat transmission rates for distinct constituents of graphene and MWCNT nanoparticles as well as changes in their ratio in the base fluid. This table shows that, as the shape components values are increased from 3.0 to 8.3, Nu increases. In addition, it is recognized that, of all the investigated combinations, hybrid nanofluid achieves the best heat transmission rate when it is made of spherical-shaped graphene nanoparticles and blade-shaped MWCNT nanoparticles, as well as brick-shaped graphene nanoparticles and spherical-shaped MWCNTs.

Table 5. The effect of volume fraction on Nusselt number and increased percent.

ϕ_{Gr}	ϕ_{MWCNT}	Pr	α	τ	Nu	% Increased
0.00	0.00	6.2	0.4	1.5	1.9721	-
0.01	0.01	6.2	0.4	1.5	1.8751	4.9
0.02	0.02	6.2	0.4	1.5	1.7850	9.5
0.03	0.03	6.2	0.4	1.5	1.7011	13.7
0.04	0.04	6.2	0.4	1.5	1.6229	17.7

Table 6. Nusselt number varies for various combinations of shape components (p_1 and p_2).

ϕ_{Gr}	ϕ_{MWCNT}	$p_1 = 3.0$				$p_2 = 3.0$			
		$p_2 = 3.7$	$p_2 = 4.9$	$p_2 = 5.7$	$p_2 = 8.3$	$p_1 = 3.7$	$p_1 = 4.9$	$p_1 = 5.7$	$p_1 = 8.3$
0.01	0.01	1.9506	1.9545	1.9562	1.9594	1.9421	1.9341	1.9301	1.9139
0.02	0.02	1.9291	1.9368	1.9402	1.9467	1.9122	1.8965	1.8888	1.8577
0.03	0.03	1.9076	1.9190	1.9241	1.9338	1.8826	1.8596	1.8482	1.8034
0.04	0.04	1.8860	1.9012	1.9079	1.9208	1.8532	1.8231	1.8085	1.7509

Table 7 portrays the impact of flow parameters on skin friction near the vertical plate. As observed here, increasing Prandtl number, ϕ_{MWCNT}, M, α, β and time leads to increase in shear stress whereas increasing ϕ_{Gr} and Gr results in decrement of shear stress.

Table 7. The influence of the various parameters on the skin friction.

ϕ_{Gr}	ϕ_{MWCNT}	Pr	α	τ	β	Gr	M	C_f
0.03	0.03	6.2	0.45	0.5	1.5	2	2	0.959525615427890
0.04	-	-	-	-	-	-	-	0.952001945188767
0.05	-	-	-	-	-	-	-	0.944169083022009
-	0.04	-	-	-	-	-	-	0.966946221691135
-	0.05	-	-	-	-	-	-	0.974469891930258
-	-	12	-	-	-	-	-	0.942932315311468
-	-	15	-	-	-	-	-	0.944117551034069
-	-	-	0.65	-	-	-	-	1.094127167925078
-	-	-	0.9	-	-	-	-	1.246661852225108
-	-	-	-	0.7	-	-	-	1.091373887426613
-	-	-	-	0.9	-	-	-	1.206821899771669
-	-	-	-	-	2.5	-	-	1.061352823595748
-	-	-	-	-	4.5	-	-	1.151739930441103
-	-	-	-	-	-	4	-	0.877486690628685
-	-	-	-	-	-	6	-	0.796478405588264
-	-	-	-	-	-	-	3	1.131848583096572
-	-	-	-	-	-	-	5	1.422179803146021

Table 8 shows the comparison of the classic and fractional approaches for various values of the Prandtl number and t = 0.5 in the temperature field. The two approaches demonstrate a high level of agreement.

Table 8. Comparison of classic and fractional approach when $\phi = 0$.

Pr	Classic Approach ($\alpha = 1$) (Soundalgekar V.M [45])	Fractional Approach ($\alpha = 0.95$)	Difference
0.71	0.3994	0.4029	0.0035
1.0	0.0082	0.0117	0.0035
1.5	0.3173	0.3234	0.0061
7.0	0.2207	0.2295	0.0088

5. Conclusions

A model for the natural convection MHD flow of generalized non-Newtonian fluid containing graphene and MWCNT nanoparticles was derived using the Caputo fractional derivatives. The outcomes of the investigated flow characteristics exhibit several remarkable behaviours that allow for further research of the various flow models. The following conclusions are brought up:

- The order of fractional derivatives can induce an increment or decrement in flow field and temperature depending on the time factor.
- In the case of cooling the plate, the fluid flow trend accelerates as the value of the Grashof number rises, whereas in the scenario of heating the plate, the reverse trend is observed.
- Heat transmission rate of water-based hybrid nanofluid with cylindrical shaped nanoparticles are 4.9%, 9.5%, 13.7% and 17.7% greater as compared to regular fluid for volume fraction $\phi = 0.01$ to 0.04, respectively.
- The blade-shaped hybrid nanoparticles are the most effective at increasing the heat transfer rate, whereas spherical nanoparticles perform at a lesser rate. These findings are significant in the long term because they help us plan for the improvement of heat transfer in cooling and heating applications.
- When compared to fluids with hybrid and non-hybrid nanofluids, fractional hybrid nanofluid shows the highest rate of heat transfer, whereas ordinary fluid shows minimum heat transmission rate. This demonstrates the fractional parameter improves fluid flow in a benchmark.

Author Contributions: Conceptualization, N.M.L. and A.G.V.; methodology, N.M.L.; software, N.M.L.; investigation, N.M.L.; writing—original draft preparation, N.M.L. and A.G.V.; writing—review and editing, N.M.L. and A.G.V. All authors have read and agreed to the published version of the manuscript.

Funding: The authors are gratefully acknowledge the Vellore Institute of Technology management for providing the necessary facilities and support to carry out this research work.

Institutional Review Board Statement: Not applicable.

Informed Consent Statement: Not applicable.

Data Availability Statement: Not applicable.

Conflicts of Interest: The authors declare no conflict of interest.

Nomenclature

u	Velocity
v	Temperature
a, b	Shape constants
Pr	Prandtl number
Gr	Grashof number
Gr	Graphene nanoparticle
$MWCNT$	Multi wall carbon nanotube

MHD	Magnetohydrodynamics
x, y	Cartesian coordinates
E_α	Mittag-Leffler function
Nu	Nusselt number
Cf	Skin friction coefficient
Greek symbols	
ρ_{nf}	Density of nanofluid $(\mathrm{Kgm^{-3}})$
$(C_p)_{nf}$	Specific heat capacity of nanofluid $(\mathrm{JKg^{-1}K^{-1}})$
$(\gamma)_{nf}$	Thermal expansion coefficient of nanofluid $(\mathrm{K^{-1}})$
κ_{nf}	Thermal conductivity of nanofluid $(\mathrm{Wm^{-1}K^{-1}})$
μ_{nf}	Dynamic viscosity of nanofluid $(\mathrm{Kgm^{-1}s^{-1}})$
σ_{nf}	Electrical conductivity of nanofluid $(\mathrm{Sm^{-1}})$
ρ_{hnf}	Density of hybrid nanofluid $(\mathrm{Kgm^{-3}})$
$(C_p)_{hnf}$	Specific heat capacity of hybrid nanofluid $(\mathrm{JKg^{-1}K^{-1}})$
$(\gamma)_{hnf}$	Thermal expansion coefficient of hybrid nanofluid $(\mathrm{K^{-1}})$
κ_{hnf}	Thermal conductivity of hybrid nanofluid $(\mathrm{Wm^{-1}K^{-1}})$
μ_{hnf}	Dynamic viscosity of hybrid nanofluid $(\mathrm{Kgm^{-1}s^{-1}})$
σ_{hnf}	Electrical conductivity of hybrid nanofluid $(\mathrm{Sm^{-1}})$
g	Specific gravity $(\mathrm{Kgm^{-3}})$
B_0	Magnetic field strength $(\mathrm{Wbm^{-1}})$
α	Fractional parameter
β	Casson parameter
τ	Time
γ	Volumetric coefficient of thermal expansion
ψ	Sphericity of nanoparticles
ϕ_1	Volume fraction of Graphene
ϕ_2	Volume fraction of MWCNTs
Subscripts	
f	Fluid
nf	Nanofluid
hnf	Hybrid nanofluid
np	Nanoparticle
w	Wall
∞	Ambient condition

References

1. Maxwell, J.C. *A Treatise on Electricity and Magnetism*; Clarendon Press: London, UK, 1873.
2. Choi, S.U.; Eastman, J.A. *Enhancing Thermal Conductivity of Fluids with Nanoparticles*; Argonne National Lab. (ANL): Argonne, IL, USA, 1995.
3. Pîslaru-Dănescu, L.; Morega, A.M.; Telipan, G.; Morega, M.; Dumitru, J.B.; Marinescu, V. Magnetic nanofluid applications in electrical engineering. *IEEE Trans. Magn.* **2013**, *49*, 5489–5497. [CrossRef]
4. Khodabandeh, E.; Safaei, M.R.; Akbari, S.; Akbari, O.A.; Alrashed, A.A. Application of nanofluid to improve the thermal performance of horizontal spiral coil utilized in solar ponds: Geometric study. *Renew. Energy* **2018**, *122*, 1–6. [CrossRef]
5. Bahiraei, M.; Hangi, M. Investigating the efficacy of magnetic nanofluid as a coolant in double-pipe heat exchanger in the presence of magnetic field. *Energy Convers. Manag.* **2013**, *76*, 1125–1133. [CrossRef]
6. Mekheimer, K.S.; Shahzadi, I.; Nadeem, S.; Moawad, A.M.; Zaher, A.Z. Reactivity of bifurcation angle and electroosmosis flow for hemodynamic flow through aortic bifurcation and stenotic wall with heat transfer. *Phys. Scr.* **2020**, *96*, 015216. [CrossRef]
7. Ayub, M.; Shahzadi, I.; Nadeem, S. A ballon model analysis with Cu-blood medicated nanoparticles as drug agent through overlapped curved stenotic artery having compliant walls. *Microsyst. Technol.* **2019**, *25*, 2949–2962. [CrossRef]
8. Siddique, I.; Sadiq, K.; Khan, I.; Nisar, K.S. Nanomaterials in convection flow of nanofluid in upright channel with gradients. *J. Mater. Res. Technol.* **2021**, *11*, 1411–1423. [CrossRef]
9. Aleem, M.; Asjad, M.I.; Shaheen, A.; Khan, I. MHD Influence on different water based nanofluids (TiO_2, Al_2O_3, CuO) in porous medium with chemical reaction and newtonian heating. *Chaos Solit. Fractals* **2020**, *130*, 109437. [CrossRef]
10. Shafiq, A.; Hammouch, Z.; Sindhu, T.N. Bioconvective MHD flow of tangent hyperbolic nanofluid with newtonian heating. *Int. J. Mech. Sci.* **2017**, *133*, 759–766. [CrossRef]
11. Yamada, A.; Sasabe, H.; Osada, Y.; Shiroda, Y.; Yamamoto, I. *Concepts of Hybrid Materials, Hybrid Materials—Concept and Case Studies*; ASM International: Novelty, OH, USA, 1989.

12. Shahzadi, I.; Bilal, S.A. Significant role of permeability on blood flow for hybrid nanofluid through bifurcated stenosed artery: Drug delivery application. *Comput. Methods Programs Biomed.* **2020**, *187*, 105248. [CrossRef]
13. Shahzadi, I.; Nadeem, S. Stimulation of metallic nanoparticles under the impact of radial magnetic field through eccentric cylinders: A useful application in biomedicine. *J. Mol. Liq.* **2017**, *225*, 365–381. [CrossRef]
14. Shahzadi, I.; Nadeem, S. A comparative study of Cu nanoparticles under slip effects through oblique eccentric tubes, a biomedical solicitation examination. *Can. J. Phys.* **2019**, *97*, 63–81. [CrossRef]
15. Javadi, H.; Urchueguia, J.F.; Mousavi Ajarostaghi, S.S.; Badenes, B. Impact of employing hybrid nanofluids as heat carrier fluid on the thermal performance of a borehole heat exchanger. *Energies* **2021**, *14*, 2892. [CrossRef]
16. Jamshed, W.; Alanazi, A.K.; Isa, S.S.; Banerjee, R.; Eid, M.R.; Nisar, K.S.; Alshahrei, H.; Goodarzi, M. Thermal efficiency enhancement of solar aircraft by utilizing unsteady hybrid nanofluid: A single-phase optimized entropy analysis. *Sustain. Energy Technol. Assess.* **2022**, *52*, 101898. [CrossRef]
17. Hafeez, M.U.; Hayat, T.; Alsaedi, A.; Khan, M.I. Numerical simulation for electrical conducting rotating flow of Au (Gold)-Zn (Zinc)/EG (Ethylene glycol) hybrid nanofluid. *Int. Commun. Heat Mass Transf.* **2021**, *124*, 105234. [CrossRef]
18. Waini, I.; Ishak, A.; Groşan, T.; Pop, I. Mixed convection of a hybrid nanofluid flow along a vertical surface embedded in a porous medium. *Int. Commun. Heat Mass Transf.* **2020**, *114*, 104565. [CrossRef]
19. Anwar, T.; Kumam, P.; Thounthong, P. A comparative fractional study to evaluate thermal performance of NaAlg–MoS_2–Co hybrid nanofluid subject to shape factor and dual ramped conditions. *Alex. Eng. J.* **2022**, *61*, 2166–2187. [CrossRef]
20. Balaji, T.; Rajendiran, S.; Selvam, C.; Lal, D.M. Enhanced heat transfer characteristics of water based hybrid nanofluids with graphene nanoplatelets and multi walled carbon nanotubes. *Powder Technol.* **2021**, *394*, 1141–1157. [CrossRef]
21. Khan, M.; Lone, S.A.; Rasheed, A.; Alam, M.N. Computational simulation of Scott-Blair model to fractional hybrid nanofluid with Darcy medium. *Int. Commun. Heat Mass Transf.* **2022**, *130*, 105784. [CrossRef]
22. Roy, N.C.; Pop, I. Analytical investigation of transient free convection and heat transfer of a hybrid nanofluid between two vertical parallel plates. *Phys. Fluids* **2022**, *34*, 072005. [CrossRef]
23. Sene, N. Analytical investigations of the fractional free convection flow of Brinkman type fluid described by the Caputo fractional derivative. *Results Phys.* **2022**, *37*, 105555. [CrossRef]
24. Khan, Z.A.; Haq, S.U.; Khan, T.S.; Khan, I.; Nisar, K.S. Fractional Brinkman type fluid in channel under the effect of MHD with Caputo-Fabrizio fractional derivative. *Alex. Eng. J.* **2020**, *59*, 2901–2910. [CrossRef]
25. Reyaz, R.; Lim, Y.J.; Mohamad, A.Q.; Saqib, M.; Shafie, S. Caputo fractional MHD Casson Fluid flow over an oscillating plate with thermal radiation. *J. Adv. Res. Fluid Mech. Therm. Sci.* **2021**, *85*, 145–158. [CrossRef]
26. Casson, N. A flow equation for pigment-oil suspensions of the printing ink type. *Rheol. Disperse Syst.* **1959**, 10021830093.
27. Raza, A.; Khan, S.U.; Farid, S.; Khan, M.I.; Sun, T.C.; Abbasi, A.; Khan, M.I.; Malik, M.Y. Thermal activity of conventional Casson nanoparticles with ramped temperature due to an infinite vertical plate via fractional derivative approach. *Case Stud. Therm. Eng.* **2021**, *27*, 101191. [CrossRef]
28. Shahrim, M.N.; Mohamad, A.Q.; Jiann, L.Y.; Zakaria, M.N.; Shafie, S.; Ismail, Z.; Kasim, A.R. Exact solution of fractional convective Casson Fluid through an accelerated plate. *CFD Lett.* **2021**, *13*, 15–25. [CrossRef]
29. Krishna, M.V.; Ahammad, N.A.; Chamkha, A.J. Radiative MHD flow of Casson hybrid nanofluid over an infinite exponentially accelerated vertical porous surface. *Case Stud. Therm. Eng.* **2021**, *27*, 101229. [CrossRef]
30. Kilbas, A.A.; Srivastava, H.M.; Trujillo, J.J. *Theory and Applications of Fractional Differential Equations*; North-Holland Mathematics Studies; Elsevier: Amsterdam, The Netherlands, 2006.
31. Caputo, M. Linear models of dissipation whose Q is almost frequency independent—II. *Geophys. J. Int.* **1967**, *13*, 529–539. [CrossRef]
32. Anwar, T.; Kumam, P. A fractal fractional model for thermal analysis of GO− NaAlg− Gr hybrid nanofluid flow in a channel considering shape effects. *Case Stud. Therm. Eng.* **2022**, *31*, 101828. [CrossRef]
33. Saqib, M.; Khan, I.; Shafie, S. Application of Atangana–Baleanu fractional derivative to MHD channel flow of CMC-based-CNT's nanofluid through a porous medium. *Chaos Solit. Fractals* **2018**, *116*, 79–85. [CrossRef]
34. Daud, M.M.; Jiann, L.Y.; Mahat, R.; Shafie, S. Application of Caputo Fractional Derivatives to the Convective Flow of Casson Fluids in a Microchannel with Thermal Radiation. *J. Adv. Res. Fluid Mech. Therm. Sci.* **2022**, *93*, 50–63. [CrossRef]
35. Ahmad, M.; Imran, M.A.; Nazar, M. Mathematical modeling of ($Cu-Al_2O_3$) water based Maxwell hybrid nanofluids with Caputo-Fabrizio fractional derivative. *Adv. Mech. Eng.* **2020**, *12*, 1687814020958841. [CrossRef]
36. Aman, S.; Zokri, S.M.; Ismail, Z.; Salleh, M.Z.; Khan, I. Casson model of MHD flow of SA-based hybrid nanofluid using Caputo time-fractional models. *Defect Diffus.* **2019**, *390*, 83–90. [CrossRef]
37. Sene, N. Analytical solutions of a class of fluids models with the Caputo fractional derivative. *Fractal Fract.* **2022**, *6*, 35. [CrossRef]
38. Nakamura, M.; Sawada, T. Numerical study on the flow of a non-Newtonian fluid through an axisymmetric stenosis. *J. Biomech. Eng.* **1990**, *112*, 100–103. [CrossRef] [PubMed]
39. Shah, N.A.; Khan, I. Heat transfer analysis in a second grade fluid over and oscillating vertical plate using fractional Caputo–Fabrizio derivatives. *Eur. Phys. J. C* **2016**, *76*, 362. [CrossRef]
40. Reddy, S.R.; Reddy, P.B. Entropy generation analysis on MHD flow with a binary mixture of ethylene glycol and water based silver-graphene hybrid nanoparticles in automotive cooling systems. *Int. J. Heat Technol.* **2021**, *39*, 1781–1790. [CrossRef]

41. Curtis, W.D.; Logan, J.D.; Parker, W.A. Dimensional analysis and the pi theorem. *Linear Algebra Its Appl.* **1982**, *47*, 117–126. [CrossRef]
42. Sene, N. Stokes' first problem for heated flat plate with Atangana–Baleanu fractional derivative. *Chaos Solit. Fractals* **2018**, *117*, 68–75. [CrossRef]
43. Abro, K.A.; Khan, I.; Gómez-Aguilar, J.F. Thermal effects of magnetohydrodynamic micropolar fluid embedded in porous medium with Fourier Sine Transform technique. *J. Braz. Soc. Mech. Sci. Eng.* **2019**, *41*, 174. [CrossRef]
44. Podlubny, I. *Fractional Differential Equations, Mathematics in Science and Engineering*; Academic Press: New York, NY, USA, 1999.
45. Soundalgekar, V.M. Free convection effect on the stokes problem for a vertical plate in an elasto-viscous fluid. *Czechoslov. J. Phys.* **1978**, *28*, 721–727. [CrossRef]